NeuroImage: Clinical 4 (2014) 743–756

Contents lists available at ScienceDirect

NeuroImage: Clinical

journal homepage: www.elsevier.com/locate/ynicl

Review

# Understanding disease processes in multiple sclerosis through magnetic resonance imaging studies in animal models

Nabeela Nathoo[a,b], V. Wee Yong[a,c], Jeff F. Dunn[a,b,c,d,*]

[a] Hotchkiss Brain Institute, University of Calgary, Calgary, Alberta, Canada
[b] Department of Radiology, University of Calgary, Calgary, Alberta, Canada
[c] Department of Clinical Neurosciences, University of Calgary, Calgary, Alberta, Canada
[d] Experimental Imaging Centre, University of Calgary, Calgary, Alberta, Canada

ARTICLE INFO

*Article history:*
Received 28 March 2014
Received in revised form 21 April 2014
Accepted 22 April 2014

*Keywords:*
Magnetic resonance imaging
Multiple sclerosis
Experimental autoimmune encephalomyelitis
Theiler's murine encephalomyelitis virus
Lysolecithin
Cuprizone

ABSTRACT

There are exciting new advances in multiple sclerosis (MS) resulting in a growing understanding of both the complexity of the disorder and the relative involvement of grey matter, white matter and inflammation. Increasing need for preclinical imaging is anticipated, as animal models provide insights into the pathophysiology of the disease. Magnetic resonance (MR) is the key imaging tool used to diagnose and to monitor disease progression in MS, and thus will be a cornerstone for future research. Although gadolinium-enhancing and $T_2$ lesions on MRI have been useful for detecting MS pathology, they are not correlative of disability. Therefore, new MRI methods are needed. Such methods require validation in animal models. The increasing necessity for MRI of animal models makes it critical and timely to understand what research has been conducted in this area and what potential there is for use of MRI in preclinical models of MS. Here, we provide a review of MRI and magnetic resonance spectroscopy (MRS) studies that have been carried out in animal models of MS that focus on pathology. We compare the MRI phenotypes of animals and patients and provide advice on how best to use animal MR studies to increase our understanding of the linkages between MR and pathology in patients. This review describes how MRI studies of animal models have been, and will continue to be, used in the ongoing effort to understand MS.



## 1. Introduction

Multiple sclerosis (MS) is an inflammatory, demyelinating and degenerative condition of the central nervous system (CNS) for which the cause is unknown. Animal models of MS have greatly enhanced knowledge of the pathophysiology of the disease. Each of these animal models provides different potential routes to investigate MS disease processes. The experimental autoimmune encephalomyelitis (EAE) model provides the opportunity to study inflammation, demyelination and axonal loss initiated by an autoimmune response to central nervous system (CNS) components. Viral models, particularly those induced by Theiler's murine encephalomyelitis virus (TMEV), enable examination of an immune response to a viral infection leading to demyelination. Demyelinating models caused by toxins such as lysolecithin, cuprizone and ethidium bromide afford the opportunity to investigate a primary demyelinating insult.

Magnetic resonance imaging (MRI) plays an integral role in the diagnosis of MS, for tracking the disease course, and for determining the effectiveness of treatments (for a review, refer to Filippi and Rocca, 2011). New MRI methods are continually being developed to provide more information about MS disease processes with the goal of improving the correlation of MRI with clinical disability. Ideally, knowledge gained from MRI studies in animal models can be translated to human studies to improve the interpretation of MRI and to inform human studies on elements of disease.

Here, we review MRI and magnetic resonance spectroscopy (MRS) studies of animal models of MS specifically with respect to investigating pathology. We relate these to what has been found in MS patients. We previously reviewed the use of MRI studies of animal models of MS for testing drugs in MS (Nathoo et al., 2014). We also discuss how MRI can be applied to answer questions about the pathophysiology of MS using animal models of MS. Such studies at the preclinical stage have the potential to direct subsequent application of MRI in the human MS population.

* Corresponding author at: Department of Radiology, University of Calgary, 3330 Hospital Drive, N.W., Calgary, Alberta T2N 4N1, Canada.
*E-mail address:* dunnj@ucalgary.ca (J.F. Dunn).

2213-1582/$ - see front matter 
http://dx.doi.org/10.1016/j.nicl.2014.04.011

## 2. MRI studies in animal models of MS

### 2.1. Experimental autoimmune encephalomyelitis (EAE)

EAE is a model of chronic inflammation and is the animal model used most often to investigate MS. Many variants of the EAE model exist that can display monophasic, relapsing–remitting, chronic-progressive or chronic-relapsing disease courses depending on the animal strain and immunogen used. Taken together, the diverse types of EAE models present the spectrum of clinical phenotypes observed in MS (Kipp et al., 2012). EAE immunization uses components of the CNS which stimulate the immune system via antigen presentation and autoimmunity. The antigen may be from CNS homogenate or purified myelin peptides, such as myelin basic protein (MBP), myelin oligodendrocyte glycoprotein (MOG), or proteolipid protein (PLP). This results in an autoimmune condition which targets myelin. EAE has been induced and examined across species with earlier studies focusing on non-human primates. Rodent models, particularly those using mice, are now more commonly used due to the affordability and availability of genetically modified murine strains (Ransohoff, 2012).

MS and EAE share several characteristics, including the destruction of myelin sheaths and axonal degeneration (Steinman and Zamvil, 2005). In addition, numerous CNS lesions are present which are distributed in space and time (Adams and Kubik, 1952; Baxter, 2007). MS and several variant models of EAE have evidence supporting a genetic susceptibility influenced by major histocompatibility complex class II haplotype (Steinman and Zamvil, 2005). Furthermore, CD4+ and CD8+ T-cells can be seen in lesions in both conditions, some of which are reactive to myelin proteins (Steinman and Zamvil, 2005). Studies have demonstrated that at the molecular level, the process of leukocyte migration into the CNS is similar in EAE to that in MS (Agrawal et al., 2011). For example, activated leukocytes roll and adhere onto endothelial cells via adhesion molecules, and then ultimately cross the glia limitans to enter the CNS parenchyma (Agrawal et al., 2006).

The vast majority of MRI studies with animal models of MS have used the EAE model. Importantly, the EAE model shows the same clinico-radiological paradox seen in MS, where MRI lesion load does not always correspond to the level of clinical disability (Wuerfel et al., 2007).

#### 2.1.1. EAE: imaging non-specific pathological changes

Key pathological processes in MS including inflammation, demyelination, axonal loss and oedema have been assessed using $T_2$-weighted imaging, where areas of injury appear hyperintense. Although $T_2$ can identify each of these processes, it cannot differentiate between them, which has made $T_2$-weighted MRI a method to characterize cumulative damage to the CNS, but not to identify the individual processes responsible for the damage.

In EAE models produced in rodents and primates, lesions have been detected using $T_2$-weighted MRI, which have been shown to correspond to inflammation, demyelination and axonal loss (DeBoy et al., 2007; Hart et al., 1998; Stewart et al., 1991). These hyperintensities on $T_2$-weighted MRI have frequently been observed in the periventricular white matter (Hart et al., 1998; Boretius et al., 2006; Kuharik et al., 1988; Verhoye et al., 1996), corresponding well with what is observed in MS (Barkhof et al., 1997). Other areas where $T_2$ hyperintensities have been seen in EAE animals include the corpus callosum (Hart et al., 1998), cerebellum (Waiczies et al., 2012) and cerebral grey matter (Hart et al., 1998), albeit much less frequently than in the periventricular white matter.

In EAE, changes in $T_2$ have been observed to precede the onset of clinical signs (Stewart et al., 1991; Waiczies et al., 2012; Karlik et al., 1990; O'Brien et al., 1987). In marmosets with EAE, $T_2$ lesions in the white matter appear to enlarge over time, with stable lesions being present during later stages of lesion evolution (Boretius et al., 2006). $T_2$ contrast does not appear to normalize, nor does lesion size decrease over the EAE disease course (Boretius et al., 2006). In addition, acute lesions are not distinguishable from older, more chronic lesions on $T_2$-weighted MRI (Kuharik et al., 1988). Interestingly, the proportion of animals where $T_2$ lesions are detected varies between studies, where the lowest proportion has been observed in rats (Dousset et al., 1999a) and guinea pigs (O'Brien et al., 1987; Dousset et al., 1992), and the highest observed in primates (Stewart et al., 1991; Hawkins et al., 1990). It is not clear if this discrepancy is attributable to species differences or to the parameters for the MRI sequence used for $T_2$. Overall, $T_2$-weighted MRI has shown similar trends in EAE as in MS.

#### 2.1.2. EAE: imaging blood brain barrier (BBB) breakdown

BBB disruption is a cardinal feature of active inflammatory lesions in MS. $T_1$-weighted MRI with gadolinium (Gd) is a component of the standard imaging protocol for MS to assess lesions with active, ongoing inflammation (Polman et al., 2011). MRI has been used to assess BBB breakdown in EAE models across species. Interestingly, the presence of Gd-enhancing lesions and Gd enhancement in general is variable amongst studies. Gd-enhancing lesions are present in EAE induced in monkeys (Hart et al., 1998; Blezer et al., 2007), dogs (Kuharik et al., 1988), guinea pigs (Cook et al., 2005; Karlik et al., 1993) and mice (Wuerfel et al., 2007; Waiczies et al., 2012; Nessler et al., 2007; Smorodchenko et al., 2007). However, Gd-enhancing lesions are not observed in some rat (Dousset et al., 1999a) and mouse (Schellenberg et al., 2007) EAE studies.

Gd-enhancing lesions have been observed in the lumbar spinal cord (Cook et al., 2005), brainstem (Wuerfel et al., 2007; Smorodchenko et al., 2007), cerebellum (Wuerfel et al., 2007; Smorodchenko et al., 2007), midbrain (Wuerfel et al., 2007) and periventricular areas (Wuerfel et al., 2007; Kuharik et al., 1988; Smorodchenko et al., 2007) (Fig. 1). BBB breakdown has been shown to take place before the presence of clinical signs in EAE mice (Wuerfel et al., 2007). Even in cases where Gd-enhancing lesions were present in EAE animals, not all of the animals showed such lesions. The percentage of EAE animals with Gd-enhancing lesions is variable, ranging from 47% in guinea pigs (Karlik et al., 1993) up to 100% in mice (Smorodchenko et al., 2007). It is likely that in EAE animals, lesions only have a disrupted BBB for a short time, and as standard time points are used for imaging, such BBB disruption may often be missed. This makes it difficult to use enhancing lesions in EAE as a biomarker of disease progression.

An interesting observation that has been made across numerous studies is that Gd enhancement occurs in areas other than in lesions (shown with histology or $T_2$-weighted MRI), including in white matter areas away from lesions (Boretius et al., 2006), in the brain parenchyma (Karlik et al., 1993), near the third ventricle (Karlik et al., 1993) and in peripheral regions of the lumbar spinal cord (Schellenberg et al., 2007). In the study with Gd enhancement in the peripheral regions of the lumbar spinal cord, histology showed that inflammatory cells appeared in the same areas which had Gd enhancement (Schellenberg et al., 2007); the co-localization of inflammation (as visualized with histology) with areas of Gd enhancement has been shown by others as well (Hawkins et al., 1990).

Although Gd has proven to be useful for detecting loss of BBB integrity in MS, Gd-enhancing MRI is not frequently used in EAE studies because changes with Gd rarely correspond with $T_2$ lesions. Instead, more sensitive tools have been proposed for assessing BBB breakdown, such as the gadolinium-based contrast agent, gadofluorine M (Gf). In rodents with EAE, Gf has been used to detect cerebral (Bendszus et al., 2008; Wuerfel et al., 2010) and spinal cord (Bendszus et al., 2008) lesions not seen with Gd or with $T_2$-weighted MRI (Bendszus et al., 2008) (Fig. 2). Gf lesions correspond well with inflammation seen via staining for macrophages/microglia (Bendszus et al., 2008; Wuerfel et al., 2010), especially in cases of severe inflammation (Bendszus et al., 2008). These studies did not comment on

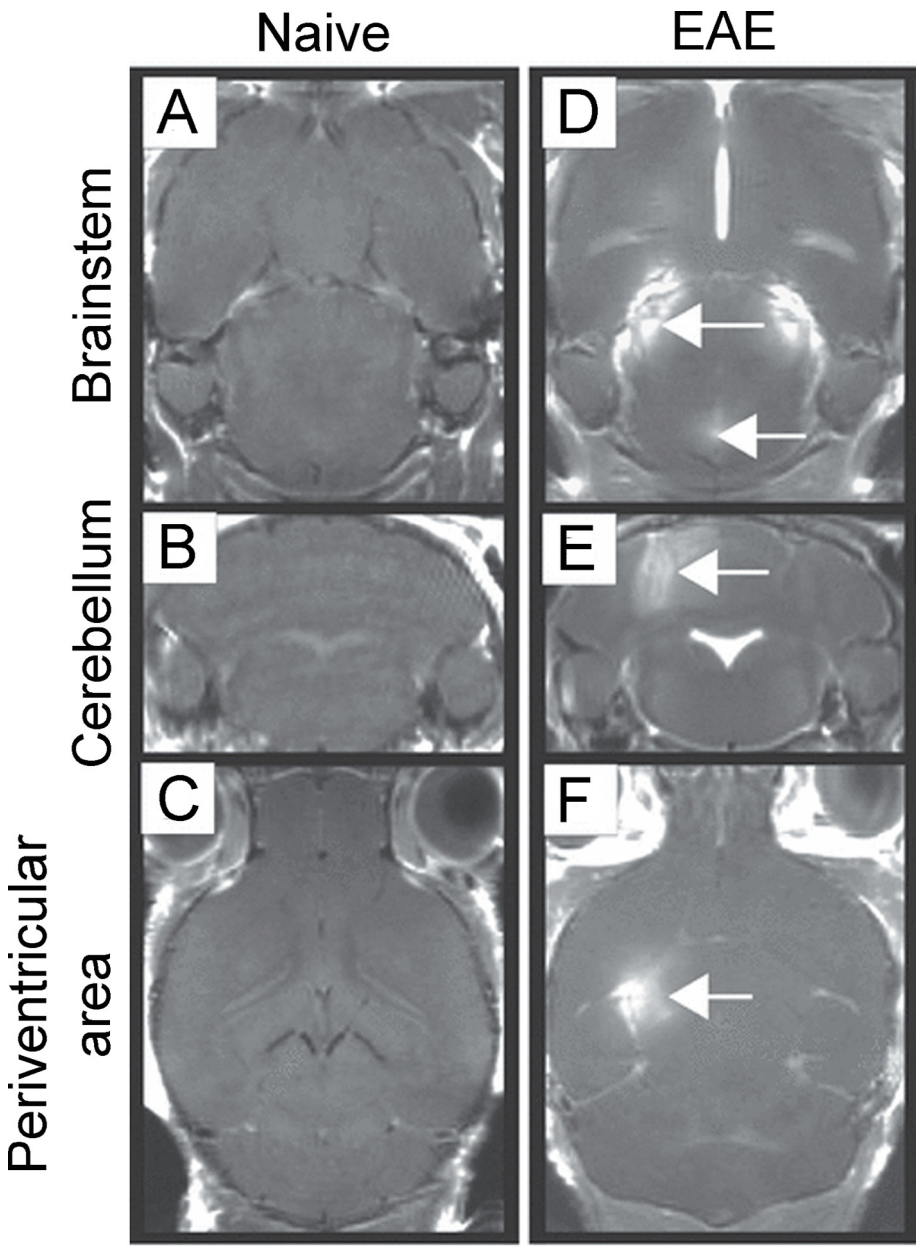


**Fig. 1.** Gadolinium (Gd)-enhancing lesions are present in the brainstem, cerebellum and periventricular area of EAE mice. (A) through (C) show images for naive mice following administration of Gd, where no enhancement is seen. (D) through (F) show images for EAE mice where Gd enhancement is seen with $T_1$-weighted imaging in the brainstem, cerebellum and periventricular area (white arrows).
(Adapted from Smorodchenko et al. (2007).)

possible co-localization between areas with Gf enhancement and the presence of lymphocytes. However, EAE lesions have a considerable presence of macrophages which may disrupt the BBB. Gf enhancement is also present in cases of inflammation of the cranial nerves in EAE mice (Wuerfel et al., 2007). In circumventricular organs, particularly in the choroid plexus, subfornicular organ and area postrema, Gf enhancement has been observed. Gf signal intensity in the subfornicular organ and area postrema was significantly correlated with EAE disease severity (Wuerfel et al., 2010). The enhanced sensitivity of Gf compared to Gd makes Gf a promising method for better detection of BBB breakdown. Importantly, in many instances, BBB breakdown is associated with inflammation, making inflammation an important process to study as well.

### 2.1.3. *EAE: imaging inflammation*

In EAE, inflammation has been studied extensively using iron oxide-based nanoparticle contrast agents. These agents provide a means to track migration of monocytes into the CNS during EAE and to follow their behaviour as macrophages once in the CNS. In EAE animals, iron nanoparticles have been shown to accumulate in the spinal cord (Chin et al., 2009; Dousset et al., 1999b; Engberink et al., 2010; Millward et al., 2013), brainstem (Chin et al., 2009; Dousset et al., 1999a; Millward et al., 2013; Brochet et al., 2006; Tysiak et al., 2009), cerebellum (Chin et al., 2009; Dousset et al., 1999a; Engberink et al., 2010; Millward et al., 2013; Brochet et al., 2006; Tysiak et al., 2009; Oweida et al., 2007), corpus callosum (Wuerfel et al., 2007), cortex (Wuerfel et al., 2007; Tysiak et al., 2009), choroid plexus (Millward et al., 2013) and vascular endothelium (Millward et al., 2013; Xu et al., 1998). In some studies, Prussian Blue staining for non-heme iron was

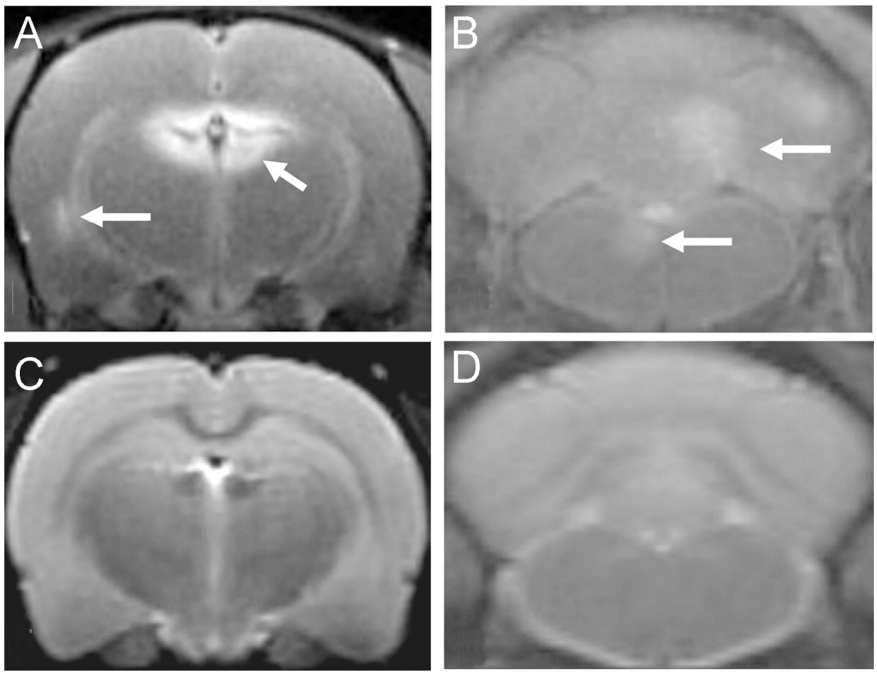


**Fig. 2.** Gadofluorine (Gf) shows contrast-enhanced lesions that are not seen using $T_2$-weighted imaging in EAE rat brain. (A) and (B) show $T_1$-weighted images of an EAE rat after Gf administration where enhancement is seen in the periventricular region, cerebellum and brainstem, respectively. (C) and (D) show corresponding $T_2$-weighted images on which the lesions are not seen.
(Adapted from Bendszus et al. (2008).)

performed to provide histological confirmation of the presence of iron nanoparticles where MRI had shown hypointense signals (Wuerfel et al., 2007; Chin et al., 2009; Engberink et al., 2010; Millward et al., 2013; Tysiak et al., 2009; Xu et al., 1998). However, staining with Prussian Blue can also indicate the presence of iron deposition unrelated to monocytes labelled with iron nanoparticles. To the best of our knowledge, monocytes labelled with iron nanoparticles have not been differentiated from iron that has been naturally deposited due to the disease process itself in any studies. In particular, one must be cautious in interpreting iron staining as sites where macrophages contain iron nanoparticles, as it is now known that iron deposition can occur in EAE mice in the lumbar spinal cord in regions of demyelination (Nathoo et al., 2013a).

Another challenge in using iron nanoparticles has been determining whether they accumulate in blood-derived macrophages or in microglia via a breached BBB. One study addressed this issue by using transgenic mice which expressed enhanced green fluorescent protein (GFP) in haematopoietic-derived macrophages, but not in microglia (Oweida et al., 2007). It was observed that regions of hypointensities on MRI in the CNS corresponded with regions that showed iron as assessed using Prussian Blue staining and with regions that were GFP-positive, indicating that the cells which had taken up the iron nanoparticles were blood-derived macrophages, not microglia (Oweida et al., 2007).

MRI using iron nanoparticles has also been used to study regional differences in lesion formation in EAE. Using $T_2$-weighted MRI, lesions (hypointense areas) were observed in the caudal part of the brainstem at disease onset, while lesions appeared in the medulla and midbrain later on in the disease course in EAE rats (Baeten et al., 2008). Hypointense areas seen in MRI correlated with areas containing macrophages as visualized using ED-1 staining (Baeten et al., 2008).

Several studies have compared monocyte infiltration into the CNS (using iron nanoparticles) and BBB breakdown (using Gd- or Gf-enhanced MRI). Most reported a discrepancy between the timing of BBB breakdown and monocyte infiltration into the CNS (Floris et al., 2004; Ladewig et al., 2009; Rausch et al., 2003), while one did not (Wuerfel et al., 2007). It has also been shown that some lesions visualized using iron nanoparticles do not correspond to Gf-enhancing lesions (Tysiak et al., 2009; Ladewig et al., 2009); this lends support to the concept that inflammatory cell transport can occur without a disrupted BBB. Thus, BBB breakdown can be due to inflammation, but inflammation does not always lead to BBB breakdown.

Others have labelled T-cells using iron nanoparticles and imaged their migration in EAE in vivo. A study that labelled CD4+ T-cells with ultrasmall superparamagnetic iron oxide (USPIO) particles observed the presence of labelled cells in the brainstem, cerebellum and frontal and prefrontal areas of the brain using $T_1$-weighted MRI with which areas of USPIO accumulation appeared hyperintense in EAE mice (Pirko et al., 2003). Other studies used MBP-reactive T-cells labelled with iron nanoparticles to induce EAE in rodents; subsequent $T_2$-weighted MRI visualized focal hypointensities in the lumbar (Robinson et al., 2010) and sacral spinal cord (Baeten et al., 2010), which corresponded to areas containing iron detected via Prussian Blue staining (Robinson et al., 2010; Baeten et al., 2010).

In one study, the locations of lesions were compared in rats that were naive when receiving labelled MBP-reactive T-cells versus those that were actively immunized for EAE when receiving labelled MBP-reactive T-cells (Baeten et al., 2010). Naive rats had hypointensities only in the sacral spinal cord, whereas primed rats had hypointensities in the brainstem, midbrain and sacral spinal cord (Baeten et al., 2010). In a different study, PLP-reactive T-cells were labelled with superparamagnetic iron oxide nanoparticles, and hypointense areas were seen in the white matter of the thoracic and lumbar spinal cord of EAE mice using $T_2$* MRI, which corresponded to areas of histologically verified inflammation and demyelination (Anderson et al., 2004) (Fig. 3).

Aside from their usage with monocytes and T-cells to study inflammation, paramagnetic contrast agents have also been tagged to antibodies directed against cell adhesion molecules which are upregulated at the level of endothelial cells at the BBB in MS (Cannella and Raine, 1995) and EAE (Cannella et al., 1990). Vascular cell adhesion

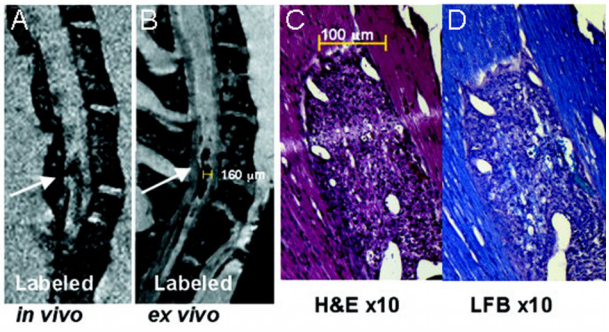


**Fig. 3.** T-cells labelled with iron nanoparticles show hypointense lesions in the spinal cord of EAE mice that correspond to areas of inflammation and demyelination. (A) and (B) show $T_2$*-weighted images of the thoracic–lumbar spinal cord in an EAE mouse, in vivo and ex vivo, respectively, where a long hypointense (dark) lesion is visible (white arrows). (C) shows haematoxylin and eosin staining, where inflammation corresponding to the lesion area is seen. (D) shows luxol fast blue staining for myelin with which demyelination is visible as a loss of blue stain.
(Adapted from Anderson et al. (2004).)

molecule-1 (VCAM-1) is one such adhesion molecule that is upregulated in MS (Battistini et al., 2003) and EAE (Steffen et al., 1994), making it a good target for studying inflammation. A VCAM-1 contrast agent based on microparticles of iron oxide (VCAM-MPIO) showed that VCAM-MPIO binding was present before the onset of clinical signs of EAE in mice (Serres et al., 2011). It was noted that binding progressed in a rostral direction over the course of EAE — before clinical signs, binding was present in the hindbrain and caudal part of the forebrain, whereas at peak disease, binding was seen throughout the forebrain (Serres et al., 2011). Knowing that VCAM-MPIO binding takes place in the brain, it would be useful to investigate the lumbar spinal cord as well. Also, VCAM-MPIO binding was observed to precede the BBB breakdown that was visualized using Gd-enhanced MRI (Serres et al., 2011). Imaging for VCAM-MPIOs has not been carried out in humans yet, but the contrast agent was not observed to have toxic effects in mice (Serres et al., 2011).

Imaging has also been carried out in EAE mice using a contrast agent for intercellular adhesion molecule-1 (ICAM-1) based on an anti-ICAM-1 antibody-conjugated paramagnetic liposome (APCL) with $T_1$-weighted MRI (Sipkins et al., 2000). Using this method, considerable increases in signal intensity were seen in the cerebellar and cerebral cortices, and ICAM-1 was upregulated on vessels both with and without infiltration of immune cells (Sipkins et al., 2000). Changes in grey matter were thought to be due to increased vascularization in the grey matter as compared to the white matter (Sipkins et al., 2000). This is supported by a study showing that angiogenesis takes place in the grey matter in EAE mice (Macmillan et al., 2011).

### 2.1.4. EAE: imaging white matter changes

Demyelination of the white matter is a common feature of MS. In EAE, white matter changes have been studied using a variety of MRI methods. However, one of the challenges is distinguishing changes due to demyelination from those attributable to inflammation. One of the MRI methods sensitive to changes in white matter, magnetization transfer ratio (MTR), is reduced in MS (Schmierer et al., 2004) and in EAE (Blezer et al., 2007; Aharoni et al., 2013; Rausch et al., 2009), suggesting a loss of tissue integrity. Myelin water imaging has also been used to visualize white matter changes in MS (Laule et al., 2004) and in EAE (Gareau et al., 2000). Upon comparing MTR and myelin water fraction obtained from myelin water imaging, it appears that MTR is sensitive to inflammation, while myelin water fraction is instead more specific for myelin content (Gareau et al., 2000). As myelin water imaging is a relatively newer technique that appears to be quite promising for characterizing white matter changes, it should

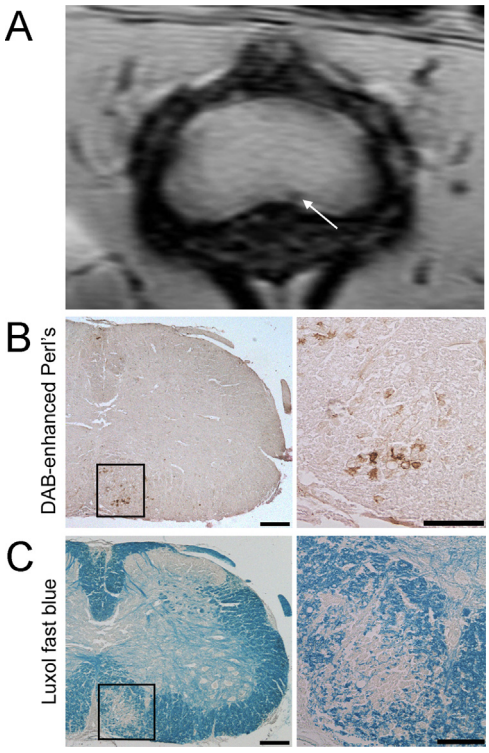


**Fig. 4.** Lesions detected in the white matter of the lumbar spinal cord of EAE mice using susceptibility-weighted imaging correspond to areas of iron deposition and demyelination. (A) shows the susceptibility-weighted MRI of the lumbar spinal cord of an EAE mouse where a lesion can be seen in the ventral white matter (white arrow). (B) shows DAB-enhanced Perl's staining for the lesion area on which iron deposits can be seen as areas of brown. (C) shows luxol fast blue staining for myelin where demyelination can be seen by the loss of blue stain.
(Adapted from Nathoo et al. (2013a).)

be explored further in EAE as well as other animal models of MS for assessing demyelination, and potentially remyelination as well.

White matter changes have also been assessed using susceptibility-weighted imaging. Lesions detected with this technique in the ventral white matter of the lumbar spinal cord of EAE mice correspond to areas of demyelination and iron deposition (Nathoo et al., 2013a) (Fig. 4).

### 2.1.5. EAE: imaging axonal damage

The magnitude of axonal loss is widely considered to be the main element responsible for a patient's transition from relapsing–remitting to secondary progressive MS (Trapp et al., 1999). Axonal damage and loss have been studied in MS using $T_1$-weighted MRI, with "black holes" or persistent hypointensities on $T_1$ being indicative of severe axonal loss (Sahraian et al., 2010). Such persistent hypointensities have also been documented using $T_1$-weighted MRI in EAE mice. This study indicated that the pathological correlate of a $T_1$ black hole was significant demyelination and inflammation and axonal loss (Nessler et al., 2007).

As diffusion is sensitive to the presence of myelin and cell organization, diffusion tensor imaging (DTI) shows promise for detecting pathology in MS. Axial diffusivity, a metric obtained by DTI, is reduced throughout all of the white matter in EAE mice (Budde et al., 2008; Budde et al., 2009), and correlates with a decrease in SMI31 staining for phosphorylated neurofilaments, indicative of axonal loss (Budde et al., 2009). In addition, changes in axial diffusivity are well correlated with clinical score in the MOG-induced EAE mouse model (Budde et al., 2009) (Fig. 5). Changes in axial diffusivity have been variable in human studies of MS, with some studies reporting a decrease (Tillema et al., 2012), others reporting an increase (Liu et al.,

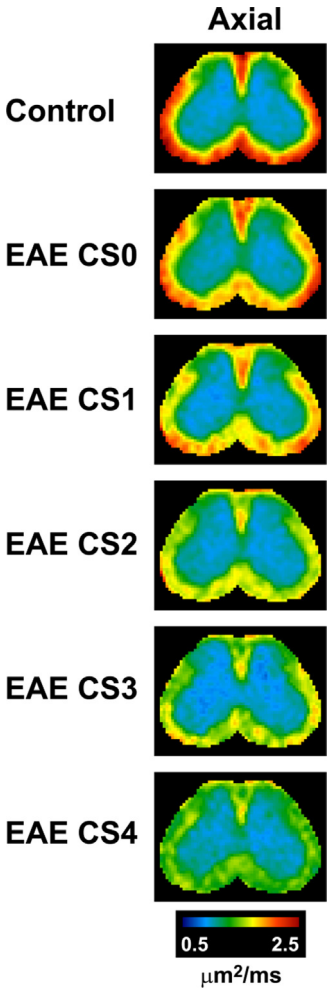


**Fig. 5.** Axial diffusivity decreases in the ventrolateral white matter and the posterior area of the dorsal white matter in the lumbar spinal cord with increasing disease severity in EAE mice. Axial diffusivity maps of the spinal cords (segment L2) of EAE animals obtained using in vivo DTI are shown where clinical scores (CS) range from 0 (least severe) to 4 (most severe). Areas with the highest axial diffusivity values are shown in red, while areas with the lowest axial diffusivity values are shown in green and blue.
(Adapted from Budde et al. (2009).)

2012), and some reporting no alteration (Naismith et al., 2010). Although some studies have shown that changes in axial diffusivity are related to axonal loss, others have made the case that axial diffusivity may not relate to axonal damage only (Harrison et al., 2013). The uncertainty between changes in axial diffusivity and MS pathology remains to be addressed.

### 2.1.6. EAE: imaging optic neuritis

Optic neuritis (ON) is characterized by inflammation and demyelination of the optic nerve and is frequently a precursor for MS, with 50% of those with ON going on to develop MS after 15 years (Optic Neuritis Study Group, 2008). ON is one of the most common initial symptoms seen in MS (Ebers, 1985). In EAE, ON has been observed in numerous studies using MRI. One study using $T_2$ and Gd-enhancing MRI showed that half of the marmosets with EAE developed ON (Boretius et al., 2006). Such enhancement of the optic nerve and optic tract has been observed by others using Gf in EAE mice (Wuerfel et al., 2007). Gf has been shown to be superior to Gd at detecting contrast enhancing lesions in the optic nerve, with nine of ten total contrast enhancing lesions in the optic nerve in EAE mice being detected using Gf, but not Gd (Wuerfel et al., 2010).

In EAE mice, damage to the optic nerve has also been observed using DTI which shows decreases in axial diffusivity and increases in radial diffusivity, believed to correspond to axonal damage and myelin damage respectively (Sun et al., 2007). Such damage to the optic nerve has also been seen in humans; mean diffusivity and radial diffusivity are elevated while fractional anisotropy is reduced in the affected optic nerve (Kolbe et al., 2009; Trip et al., 2006). Taken together, these studies indicate a loss of tissue integrity. The increase in radial diffusivity in the optic nerve seen in EAE parallels that seen in humans. However, in humans with optic neuritis, axial diffusivity is elevated in the affected optic nerve (Kolbe et al., 2009), which contradicts what has been seen in EAE — the possible reasons for this require further investigation.

### 2.1.7. EAE: imaging atrophy

CNS atrophy is another key MS disease process which has been studied in EAE. However, fewer studies have been carried out than expected in this area in EAE considering that grey matter atrophy is perhaps best correlated with clinical disability in MS (Tedeschi et al., 2005). Furthermore, atrophy appears to be accelerated when one is transitioning between stages of MS. When converting from clinically isolated syndrome to relapsing–remitting MS, grey matter atrophy is 3.4 fold greater than normal (Fisher et al., 2008); when transitioning from relapsing–remitting MS to secondary progressive MS, grey matter atrophy is 12.4 fold greater than normal (Fisher et al., 2008).

Using $T_2$-weighted MRI in models of EAE induced with MOG in mice, atrophy has been shown to take place in the cerebellar (MacKenzie-Graham et al., 2006; MacKenzie-Graham et al., 2009) and cerebral cortices (MacKenzie-Graham et al., 2012); atrophy is also present at the level of the whole brain (MacKenzie-Graham et al., 2012). Volume changes in EAE mice are related to cumulative disease score when studying the cerebellum, but not at the level of the whole brain (MacKenzie-Graham et al., 2012). In the cerebellar cortex, atrophy was linked to apoptosis of Purkinje cells (MacKenzie-Graham et al., 2009). An inverse correlation was also present between cerebellar volume and disease duration, suggesting that as the disease progresses, atrophy develops (MacKenzie-Graham et al., 2009).

Atrophy has also been shown in EAE by measuring ventricle volume, where lateral ventricle volume was two to seven fold larger in EAE mice induced using PLP than in controls (Aharoni et al., 2013). However, such an increase in lateral ventricle volume was less pronounced in EAE mice induced using MOG (Aharoni et al., 2013), suggesting that different CNS antigens can produce variations in EAE pathology.

### 2.1.8. EAE: imaging vascular changes

Vascular alterations and abnormalities have been observed in MS for a number of years (Adams, 1988). This is a significant area of investigation as many lesions in MS are centred on venous vessels, and it has recently been suggested that the presence of a central vein in a lesion has strong predictive value for an MS diagnosis (Mistry et al., 2013). Vascular abnormalities have been observed as large hypointense vessels in pre-contrast $T_2^*$ MRI in EAE mice (Xu et al., 1998). Lesions have also been observed in association with intracortical vessels with $T_2^*$ in EAE mice (Waiczies et al., 2012). In the same study, venous abnormalities were seen in the brains of three of seven EAE mice using susceptibility-weighted imaging, either the day before or on the day of onset of motor disability (Waiczies et al., 2012). Another study showed that many hypointensities detected using susceptibility-weighted imaging in the lumbar spinal cord and cerebellum of EAE mice were due to intravascular deoxyhaemoglobin, which was determined by imaging animals before and after perfusion of blood. These signal changes were region specific, localizing to the grey/white matter boundary in the spinal cord and to white matter tracts in the cerebellum (Nathoo et al., 2013a) (Fig. 6). Vessels in the

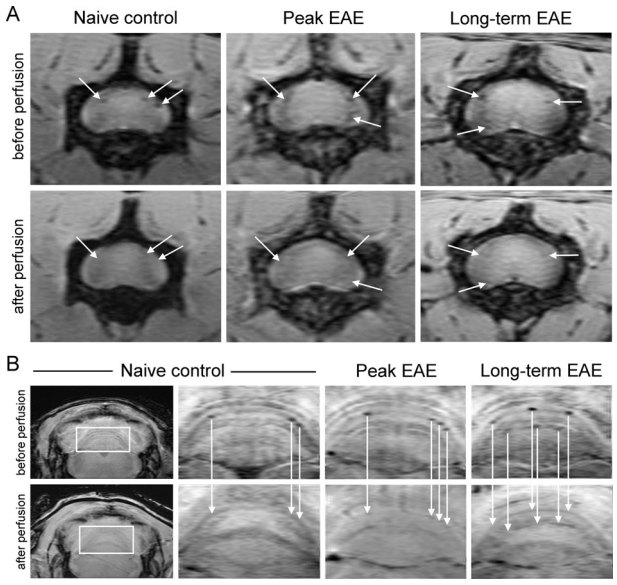


**Fig. 6.** Vascular lesions due to intravascular deoxyhaemoglobin can be detected using susceptibility-weighted imaging in EAE mice. (A) shows hypointense spots around the grey/white matter boundary and pia mater of the lumbar spinal cord seen in vivo (before perfusion) which disappear after perfusion (white arrows). (B) shows hypointense spots in the white matter tracts of the cerebellum observed in vivo (before perfusion) which disappear after perfusion (white arrows). Taken together, these data indicate that many hypointensities detected with susceptibility-weighted imaging in EAE mice are due to deoxyhaemoglobin in blood vessels.
(Adapted from Nathoo et al. (2013a).)

cerebellum also showed significant perivascular cuffing (Nathoo et al., 2013a).

One study used 2D time-of-flight MR angiography to show that the branch positions of arteries in the lumbar spinal cord of EAE mice were altered (shifting more towards the caudal direction of the spinal cord), but these observations were not confirmed with histology (Mori et al., 2014).

#### 2.1.9. EAE: imaging functional changes

Alterations in axonal connection and function have been detected in EAE using fMRI, in the form of manganese-enhanced MRI (MEMRI) (Chen et al., 2008), where manganese contrast tracks along axons with functionally connected synapses. In EAE rats, neuronal dysfunction observed using MEMRI was independent of myelin and axonal damage (Chen et al., 2008); this observation contrasts that seen in MS where changes in functional connectivity and structural white matter damage are related (Ceccarelli et al., 2010). However, fMRI studies in MS have used only BOLD MRI, not MEMRI, due to the neurotoxicity of manganese (Silva and Bock, 2008). To the best of our knowledge, no studies have been conducted using BOLD MRI in EAE.

#### 2.1.10. EAE: imaging metabolites

Using MRS, changes in metabolites have been studied in EAE. $^{1}$H-MRS measures metabolites including n-acetylaspartate (NAA), choline, myoinositol, lactate and glutamate. Studies using $^{1}$H-MRS in EAE have consistently come to the conclusion that NAA, a neuronal marker, is reduced in EAE (Chen et al., 2008; Brenner et al., 1993; Preece et al., 1993; Richards et al., 1995). This is in agreement with the finding in MS of reduced NAA at the level of the whole brain (Rigotti et al., 2012) and in the normal-appearing white matter (Aboul-Enein et al., 2010). Increased levels of choline and choline metabolites have also been seen in EAE (Brenner et al., 1993; Preece et al., 1993; Richards et al., 1995), as in MS (Inglese et al., 2003; Tartaglia et al., 2002), indicative of increased membrane turnover (Lin et al., 2005). Increases in the ratio between phosphocreatine and total

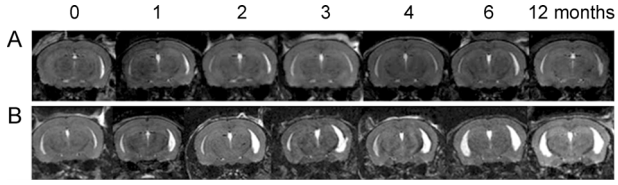


**Fig. 7.** Mice with TMEV develop ventricular enlargement concurrently with disease progression as seen using $T_2$-weighted imaging with 3D MRI datasets. (A) shows the brain of a normal mouse where no ventricular enlargement is seen over the span of 12 months. (B) shows the brain of a mouse with TMEV where ventricular enlargement can be seen on both the right and left sides, which gets progressively worse the longer the animal has the disease.
(Adapted from Pirko et al. (2011).)

$^{31}$P (Husted et al., 1994) and in the ratio between phosphocreatine and β-adenosine triphosphate (Minderhoud et al., 1992) have been observed in MS patients using $^{31}$P-MRS, suggestive of alterations in energy metabolism; $^{31}$P-MRS has not yet been carried out in EAE.

### 2.2. Theiler's murine encephalomyelitis virus (TMEV)

TMEV is a member of the Picornaviridae family of RNA viruses. Administering TMEV intracerebrally in susceptible mouse strains (like SJL/J) leads to demyelination (Dal Canto et al., 1996; Denic et al., 2011). Typically the disease is either monophasic or biphasic — the biphasic condition shows chronic demyelination (presenting as chronic-progressive), leading to the development of spinal cord lesions, similar to those observed in EAE (Dal Canto et al., 1996; Denic et al., 2011).

#### 2.2.1. TMEV: imaging changes in deep grey matter

$T_2$ hypointensity in the deep grey matter of the brain has been observed in mice with TMEV which develops as the disease progresses. There is strong correlation between the degree of $T_2$ hypointensity and impaired motor function (Pirko et al., 2009). TMEV is the only animal model of MS in which such MRI-detectable deep grey matter changes have been shown. This observation is significant, as the phenomenon of abnormalities in deep grey matter structures is commonly observed in MS using MRI, and has been shown to be related to disease duration and grey matter atrophy (Khalil et al., 2009). Corresponding histological data have shown that these MRI changes in MS patients are due to excess iron deposition (Walsh et al., 2013). It is not currently known if MRI-detectable deep grey matter abnormalities in TMEV are due to iron deposition.

#### 2.2.2. TMEV: imaging atrophy

As is the case in EAE, brain atrophy has been studied in TMEV. In mice with TMEV, atrophy via ventricular enlargement has been observed using $T_2$-weighted imaging 3 months into the disease course and peaked at 6 months (Pirko et al., 2011) (Fig. 7). Atrophy was strongly correlated with impaired motor function (Pirko et al., 2011). It is interesting to note that brain atrophy is present in TMEV and in EAE, whereas brain lesions are usually less common than spinal cord lesions in both of these models (Pirko et al., 2011).

#### 2.2.3. TMEV: imaging inflammation

Inflammation has been investigated in TMEV using MRI. Studies with Gd were carried out using interferon-gamma receptor knockout mice, as they develop brain lesions (Pirko et al., 2004a). Utilization of this knockout allowed for a phenotype more similar to MS than typical TMEV presentation, where lesions localize primarily to the spinal cord. Gd enhancement was not observed for every lesion; when observed, enhancement was seen early, but not late during the evolution of lesions, and never lasted longer than 7 days (Pirko et al., 2004a). Furthermore, four types of lesions were observed using $T_2$:

1) expanding lesions, 2) expanding–retracting lesions, 3) fluctuating lesions and 4) stable lesions, with expanding lesions being the most common type to show Gd-enhancement (Pirko et al., 2004a). In addition, USPIOs have been used in TMEV to track inflammation and migration of specific cell types, including CD8+ T-cells and CD4+ T-cells (Pirko et al., 2004b).

#### 2.2.4. TMEV: imaging black holes

Another interesting pathological feature of MS investigated in TMEV is the formation of hypointensities in $T_1$, or "black holes," which are related to axonal loss (Pirko et al., 2004c). However, unlike the persistent black holes occasionally observed in MS (Bagnato et al., 2003), $T_1$ black holes observed in TMEV in the periventricular and parahippocampal areas resolved by 45 days into the disease (Pirko et al., 2004c). It is possible that $T_1$ hypointensities seen in TMEV are similar in nature to acute black holes seen in MS which typically resolve within 2 months after enhancement is no longer present (Zhang et al., 2011). Interestingly, these $T_1$ black holes had reduced NAA/creatine ratios as seen using MRS which normalized at the same time black holes disappeared on $T_1$ (Pirko et al., 2004c). In a later study, the cause of $T_1$ hypointensities in TMEV was determined to be due to CD8+ T cells by virtue of their expression of perforin (Pirko et al., 2008), which creates a pore in the plasma membrane, eventually leading to cell death (Stepp et al., 2000).

#### 2.2.5. TMEV: imaging neuronal loss

Neuronal loss has been detected in the hippocampi of mice infected intracranially with TMEV. Regions with neuronal loss appeared as hyperintensities on $T_2$-weighted MRI, which also had reduced NAA as seen with $^1$H-MRS; it was specifically the CA1 layer where neurons were lost, as confirmed by histology (Buenz et al., 2009).

#### 2.2.6. TMEV: imaging white matter changes

Although $T_2$ hyperintensities have been shown in the TMEV model which are presumed to relate to demyelination, there have not been any discussions linked to these hyperintensities being linked to demyelination specifically (Pirko et al., 2004a). Histopathology has shown spinal cord lesions with demyelination in the TMEV model (Dal Canto and Lipton, 1975). Thus, more studies need to be conducted with MRI to specifically investigate white matter changes in TMEV.

### 2.3. Cuprizone

The cuprizone model is often employed to study specific aspects related to demyelinating and remyelinating events in MS. Cuprizone is a copper chelator which, when consumed in an animal's diet, produces demyelination in the corpus callosum and superior cerebellar peduncles (Blakemore, 1973; Matsushima and Morell, 2001); cortical demyelination has also been observed (Skripuletz et al., 2008). Acute demyelination involves ingestion of cuprizone for 6 weeks followed by a normal diet for 6 weeks. This paradigm leads to demyelination followed by spontaneous remyelination (Matsushima and Morell, 2001). Chronic demyelination results if cuprizone ingestion takes place for 12 consecutive weeks (Matsushima and Morell, 2001).

One advantage of the cuprizone model for imaging studies is the simplicity of the disease induction. It is a good model to follow both acute and chronic demyelination, and enables investigations of the effects of oligodendrocyte apoptosis (Matsushima and Morell, 2001).

#### 2.3.1. Cuprizone: imaging white matter changes

In cuprizone, the main processes studied using MRI have been demyelination and remyelination. Using DTI, it has been observed that radial diffusivity increases during demyelination (Song et al., 2005; Sun et al., 2006; Xie et al., 2010) and decreases with remyelination (Song et al., 2005). Changes in radial diffusivity have been shown to correspond with histological changes in myelin (Sun et al., 2006). A study comparing in vivo and ex vivo DTI in cuprizone found that ex vivo radial diffusivity was more reliable for assessing demyelination than in vivo radial diffusivity (Zhang et al., 2012). Diffusion basis spectrum imaging, a method that can detect pathology missed with DTI, has been used in cuprizone, finding that radial diffusivity derived from diffusion basis spectrum imaging had greater correlation with histology for myelin than radial diffusivity derived from DTI (Wang et al., 2011). In addition, diffusion basis spectrum imaging detected demyelination in the middle segment of the corpus callosum which was missed with DTI (Wang et al., 2011). As diffusion basis spectrum imaging is a relatively newer method, more studies should be carried out comparing this with DTI in the cuprizone model.

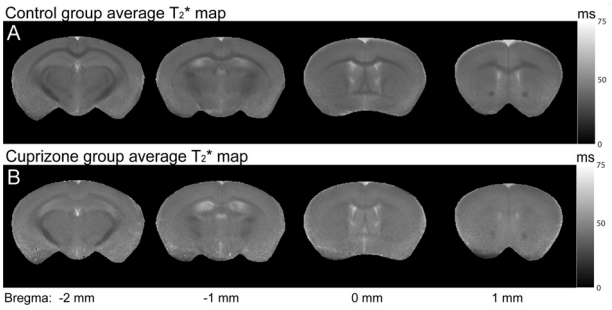


**Fig. 8.** Cuprizone-treated mice have elevated $T_2$* values and significantly reduced-grey–white matter contrast in the cortex and corpus callosum compared to control mice. (A) shows $T_2$* maps for control mice obtained ex vivo. $T_2$* values are shorter (darker on $T_2$* maps) in the cortex and corpus callosum of controls compared to images shown in (B) which are the $T_2$* maps for cuprizone-treated mice obtained ex vivo. Also, grey–white matter contrast is reduced in cuprizone-treated mice compared to control mice.
(Adapted from Lee et al. (2012).)

Magnetization transfer imaging (MTI) has also been used for monitoring changes in white matter following cuprizone intoxication. MTR was significantly decreased during demyelination and increased with remyelination in the cuprizone model (Zaaraoui et al., 2008). These changes were strongly correlated with histology for myelin (Zaaraoui et al., 2008). An interesting approach for characterizing the status of myelin in cuprizone was carried out using $T_1$, $T_2$ and MTR, with the combined use of these three methods showing up to 95% prediction strength in establishing the myelin status of a lesion (Merkler et al., 2005). This combined approach fared well in distinguishing demyelination from remyelination (Merkler et al., 2005). Another study used $T_1$, multi-component $T_2$, DTI and quantitative MTI in mice exposed to cuprizone for up to 6 weeks (Thiessen et al., 2013). Fractional anisotropy was significantly reduced while mean, axial and radial diffusivities were significantly increased. In addition, signal intensity in $T_2$ was significantly elevated and MTR was significantly reduced in the corpus callosum. With quantitative MTI, the transfer rate between the bound and free pools (k) and the bound pool fraction (f) were significantly decreased in the corpus callosum and external capsule; there was a significant correlation between f and the myelin sheath fraction (Thiessen et al., 2013), suggesting that a reduction in f is related to myelin loss. Using $T_2$* in cuprizone, it has been observed that demyelination leads to significantly increased $T_2$* in white matter while there is a drastic decrease in grey–white matter frequency contrast, indicating that myelin is the major source of such frequency contrasts (Lee et al., 2012) (Fig. 8).

#### 2.3.2. Cuprizone: imaging changes in deep grey matter

A study recently investigated demyelination in deep grey matter structures in cuprizone using MTI, finding that MTR values decreased significantly in cuprizone mice compared to controls. MTR decreased by 0.39% each week of cuprizone exposure (6 weeks), but increased

after ending cuprizone treatment (for 2 weeks). MTI results showed a significant weak positive correlation with staining for myelin using PLP immunohistochemistry (Fjaer et al., 2013). These results are significant as deep grey matter demyelination has been shown to take place in MS with histopathology (Vercellino et al., 2009).

#### 2.3.3. Cuprizone: imaging axonal damage

Axonal damage has been studied in cuprizone using MRI. With diffusion weighted imaging, reduced parallel apparent diffusion coefficient was observed with cuprizone treatment in the caudal part of the corpus callosum (Wu et al., 2008). Furthermore, a positive correlation was observed between parallel apparent diffusion coefficient and neurofilament staining, indicative of axonal density (Wu et al., 2008).

Using in vivo DTI, axial diffusivity was shown to be a better indicator of axonal injury compared with ex vivo axial diffusivity (Zhang et al., 2012). Axial diffusivity has been shown to be reduced at the 4 week time point, which has been supported by histology for axonal damage (Sun et al., 2006). Another study corroborated that axial diffusivity was reduced during the acute phase of cuprizone demyelination (up to 6 weeks), but that this correlation was lost after the 6 week time point (Xie et al., 2010). More studies need to be conducted to assess axial diffusivity during the chronic demyelinating phase. Taken together, these studies support the use of in vivo axial diffusivity as a marker of axonal injury during the acute demyelinating phase in the cuprizone model.

### 2.4. Lysolecithin

The lysolecithin model produces a demyelinating lesion via injection of an activator of phospholipase A2, lysophosphatidylcholine, into a specific area in the CNS which may include the dorsal and ventral columns of the spinal cord, corpus callosum and internal capsule (Denic et al., 2011). The lysolecithin model involves demyelination and remyelination which follows a known disease course lasting roughly 1 month. From an imaging perspective, this model is excellent for validating methods that detect demyelination and remyelination.

#### 2.4.1. Lysolecithin: imaging white matter changes

Studies using MTI have shown a reduction in MTR with demyelination in rodents and monkeys (Deloire-Grassin et al., 2000; Dousset et al., 1995; McCreary et al., 2009). However, there is variation on how MTR changes with remyelination, with one study citing that MTR increases with remyelination in lysolecithin-injected rats (Deloire-Grassin et al., 2000), while the other using lysolecithin-injected mice did not observe a significant change in MTR over the disease course after the 14 day time point (McCreary et al., 2009). These studies share the observation that MTR values do not return to the values observed at baseline which is supported by histology indicating incomplete remyelination (Deloire-Grassin et al., 2000; McCreary et al., 2009). That there is disagreement between studies on how MTR changes when remyelination takes place indicates that this area needs to be investigated further.

Myelin water fraction has been used alongside MTR, where it was observed that values returned to baseline by 28 days after injection (the time point at which remyelination would be as close to complete as possible), while MTR values did not return to baseline (McCreary et al., 2009). It is known, based on histology, that while remyelination does take place in this model, it is not complete (Blakemore, 1978). Therefore, it is worth investigating why myelin water fraction returns to baseline when it is known that remyelination is incomplete.

Diffusion weighted imaging has also been applied to the lysolecithin model. The apparent diffusion coefficient was elevated in the region surrounding the lesion compared to the lesion area itself early on in the disease course, which was attributable to oedema (Degaonkar et al., 2002). This observation of early oedema has been replicated in another study using diffusion weighted imaging (Tourdias et al., 2011). Upon remyelination, apparent diffusion coefficient values in the lesion area and in the area surrounding the lesion were dramatically reduced (Degaonkar et al., 2002). Using DTI, fractional anisotropy and axial diffusivity are shown to decrease while radial diffusivity increases in lysolecithin-injected rats (DeBoy et al., 2007). Tractography, which provides a visual representation of white matter tracts with DTI, has shown that the lesion area at the time of maximum demyelination in lysolecithin appears to have a loss of white matter tracts (Nathoo et al., 2013b) (Fig. 9). Taken together, methods that have been used to investigate white matter changes over the lysolecithin disease course are promising, but further work needs to be done to identify which method(s) can reliably provide a measure of remyelination and repair.

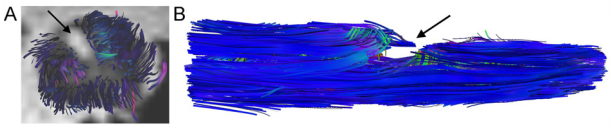


**Fig. 9.** Tractography obtained using diffusion tensor imaging shows a lysolecithin lesion in mouse spinal cord with a loss of white matter tracts at 7 days post-injection. (A) shows a lysolecithin spinal cord in the axial orientation 7 days post-injection, where the lesion area is bright on the image and does not appear to contain white matter tracts (black arrow). The surrounding spinal cord area has tracts projecting from it. (B) shows the same spinal cord lengthwise, where the lesion area is visible as a large gap (black arrow).
(Adapted from Nathoo et al. (2013b).)

#### 2.4.2. Lysolecithin: imaging BBB breakdown

The BBB breakdown that would typically accompany oedema in the lysolecithin model has also been studied using Gd. There appears to be controversy as to whether lysolecithin lesions show enhancement with Gd which would be indicative of BBB breakdown. One study reported no Gd enhancement in lysolecithin-injected monkeys (Dousset et al., 1995), while another reported Gd enhancement in early lesions in lysolecithin-injected rats (Ford et al., 1990). A recent study which incorporated Evans blue staining for BBB permeability showed that the BBB is compromised early in the lysolecithin disease course, which resolved later in the disease course, at approximately the same time as oedema declined (Tourdias et al., 2011). With only a few studies conducted in this area using MRI and given their differing results, it would be useful to examine BBB breakdown in this model further.

### 2.5. Imaging of other animal models used to study MS

In the realm of animal work in MS, there is always the possibility of creating new animal models, or combining established animal models to give a new phenotype. One study combined EAE and cuprizone, using DTI to assess pathology. Primary demyelination after cuprizone led to changes in radial diffusivity, but not axial diffusivity (Boretius et al., 2012). However, mice with demyelination, inflammation and axonal damage showed less drastic changes in radial diffusivity (Boretius et al., 2012). Therefore, it is possible that radial diffusivity serves as a good marker of demyelination alone, but when other disease processes are present, as is the case in MS, it is less useful. The observation that radial diffusivity is useful in cases of a primary demyelinating insult has also been made using DTI in the lysolecithin model (Nathoo et al., 2013b).

There is also the possibility of studying MS disease processes using transgenic mice that show certain MS disease processes without active induction of disease. One such model involves using the ND4 mouse that has many copies of the DM-20 isoform of PLP, which leads to spontaneous demyelination at around 3 months of age (Mastronardi et al., 1993). Using $T_2$ in this model, demyelination was observed in the corpus callosum and cerebellum starting at

**Table 1**
Summary of pathologies and MRI phenotypes in animal models of MS.

| Animal model | Pathology | MRI method(s) and phenotype | References |
|---|---|---|---|
| EAE | BBB breakdown | Enhancement with Gd | Wuerfel et al. (2007), Hart et al. (1998), Kuharik et al. (1988), Waiczies et al. (2012), Blezer et al. (2007), Cook et al. (2005), Karlik et al. (1993), Nessler et al. (2007), and Smorodchenko et al. (2007) |
| | | Enhancement with Gf | Bendszus et al. (2008) and Wuerfel et al. (2010) |
| | Inflammation | Hypointensities with $T_2$- or $T_2$*-weighted MRI or hyperintensities in $T_1$-weighted MRI in combination with iron nanoparticles | Wuerfel et al. (2007), Chin et al. (2009), Dousset et al. (1999a), Engberink et al. (2010), Millward et al. (2013), Brochet et al. (2006), Tysiak et al. (2009), Oweida et al. (2007), and Xu et al. (1998) |
| | White matter changes | Decrease in MTR | Blezer et al. (2007), Aharoni et al. (2013), and Rausch et al. (2009) |
| | Axonal damage | Black holes on $T_1$-weighted MRI | Nessler et al. (2007) |
| | | Decrease in axial diffusivity with DTI | Budde et al. (2008) and Budde et al. (2009) |
| | Optic neuritis | Hyperintensity on $T_2$-weighted MRI | Boretius et al. (2006) |
| | | Enhancement with Gd or Gf | Wuerfel et al. (2007), Boretius et al. (2006), and Wuerfel et al. (2010) |
| | | Decrease in axial diffusivity and increase in radial diffusivity with DTI | Sun et al. (2007) |
| | Atrophy | Cerebellar cortical atrophy, cerebral cortical atrophy and whole brain atrophy with $T_2$-weighted MRI | MacKenzie-Graham et al. (2006), MacKenzie-Graham et al. (2009), and MacKenzie-Graham et al. (2012) |
| | Vascular changes | Hypointensities with $T_2$*-weighted MRI and susceptibility-weighted MRI | Waiczies et al. (2012), Xu et al. (1998), and Nathoo et al. (2013a) |
| | | 2D time-of-flight angiography for altered branch positions of spinal arteries | Mori et al. (2014) |
| | Functional changes | Neuronal dysfunction with MEMRI | Chen et al. (2008) |
| | Changes in metabolites | Reduction in NAA with $^1$H-MRS | Chen et al. (2008), Brenner et al. (1993), Preece et al. (1993), and Richards et al. (1995) |
| TMEV | BBB breakdown and inflammation | Hyperintensities on $T_2$-weighted MRI and enhancement with Gd | Pirko et al. (2004a) |
| | Atrophy | Ventricular enlargement with $T_2$-weighted MRI | Pirko et al. (2011) |
| | Black holes | Hypointensities with $T_1$-weighted MRI that resolve during the disease course | Pirko et al. (2004c) |
| | Changes in deep grey matter | Hypointensity on $T_2$-weighted MRI | Pirko et al. (2009) |
| | Neuronal loss | Hyperintensities on $T_2$-weighted MRI and reduction in NAA with $^1$H-MRS | Buenz et al. (2009) |
| | White matter changes | Hyperintensities have been seen on $T_2$-weighted MRI, but have not been discussed with respect to demyelination specifically | Pirko et al. (2004a) |
| | | Histology shows demyelination in spinal cord lesions | Dal Canto and Lipton (1975) |
| Cuprizone | White matter changes | Increase in radial diffusivity, increase in axial diffusivity and decrease in fractional anisotropy with DTI with demyelination | Song et al. (2005), Sun et al. (2006), Xie et al. (2010), and Thiessen et al. (2013) |
| | | Decrease in MTR with demyelination | Zaaraoui et al. (2008), Merkler et al. (2005), and Thiessen et al. (2013) |
| | | Increase in $T_2$* and decrease in grey-white matter frequency contrast with demyelination | Lee et al. (2012) |
| | Axonal damage | Reduced parallel apparent diffusion coefficient with DWI | Wu et al. (2008) |
| | | Decrease in axial diffusivity with DTI | Sun et al. (2006), Xie et al. (2010), and Zhang et al. (2012) |
| | Changes in deep grey matter | Decrease in MTR | Fjaer et al. (2013) |
| Lysolecithin | BBB breakdown | Enhancement with Gd | Ford et al. (1990) |
| | White matter changes | Decrease in MTR with demyelination | Deloire-Grassin et al. (2000), Dousset et al. (1995), and McCreary et al. (2009) |
| | | Decrease in axial diffusivity and fractional anisotropy and increase in radial diffusivity with DTI with demyelination | DeBoy et al. (2007) |

5 months of age (Enriquez-Algeciras et al., 2011).

## 3. Summary of MRI results across animal models of MS

In summary, a variety of MRI methods have been used to study a wide range of pathologies across the key animal models used to study MS — EAE, TMEV, cuprizone and lysolecithin. The EAE model is the most extensively studied, which may be one of the reasons that such diverse pathology has been reported. All of the animal models show white matter damage. Observations are summarized below (Table 1).

## 4. Incorporation of MRI into animal model studies of MS to increase understanding of MS pathology

MRI studies of models of MS have specific and obvious advantages. One advantage is the ability to image before and during disease progression in an individual animal. As a result, changes may be followed over time, ultimately reducing animal numbers and enabling one to compare within a single animal with statistics (Nathoo et al., 2014).

A significant benefit of using MRI in animal model studies is that it allows for the development of methods that can be translated to clinical use. This includes the development of MRI sequences and new contrast agents. Examples of new contrast agents that are not yet approved in humans include Gf and contrast agents based on VCAM-1 and ICAM-1. In EAE, Gf has shown areas of disrupted BBB (Bendszus et al., 2008; Wuerfel et al., 2010). Although Gd-enhanced MRI is currently the gold standard for assessing BBB breakdown with MRI in MS, Gf has been demonstrated to be more sensitive than Gd for this purpose (Stoll et al., 2009).

One of the contrast agents initially used in EAE that has been translated for use in MS patients is the iron-based USPIOs. Studies in EAE comparing BBB breakdown (using Gd or Gf) with infiltration of monocytes into the CNS (using USPIOs) have been particularly instructive, as they have commonly observed that there appears to be a mismatch between BBB breakdown and monocyte migration into the CNS (Floris et al., 2004; Ladewig et al., 2009; Rausch et al., 2003). Furthermore, some lesions are only detected using USPIOs in EAE (Tysiak et al., 2009; Ladewig et al., 2009). In recent years, studies have been carried out in MS patients comparing Gd with USPIOs (Dousset et al., 2006; Tourdias et al., 2012; Vellinga et al., 2008). Remarkably, these human studies have come to the same conclusion as animal studies — USPIOs may be present in areas that appear to have an intact BBB as they do not show Gd-enhancement (Dousset et al., 2006; Tourdias et al., 2012; Vellinga et al., 2008).

One of the greatest advantages of using animal models is the ability to correlate MRI metrics with histopathology to validate the sensitivity and specificity of imaging methods. This allows for improved interpretation of MRI findings in patient studies. An example of an instance where MRI has been combined with histopathology to validate the substrates seen in MRI is in the usage of susceptibility-weighted imaging in the EAE model. Iron accumulation is an aspect of MS pathophysiology, and animal imaging in combination with pathological analysis has verified that susceptibility-weighted imaging can detect tissue iron (Nathoo et al., 2013a) which has also been observed in MS (Hopp et al., 2010). It would be beneficial to increase the number of such studies, although some may argue that correlating MRI with histology is too challenging. In fact, this is relatively easy to do within a useful range of spatial accuracy. Histological sections can easily be prepared at 10 μm in thickness or less, while the usual slice thickness for MRI is 500–1000 μm. Therefore, with serial sectioning, a histological section can easily be localized within an MRI slice using anatomical markers. With the inevitable limitations faced in obtaining human MS tissue at various stages of disease progression, more animal imaging studies using histology as a correlate need to be conducted. However, one has to be wary that animal models do not mimic all aspects of MS accurately.

Animal models are continuing to develop, including models which are more specific to either subsets of MS pathology, or to MS pathophysiology as a whole. As these evolve, they will need to be studied with MRI to determine how the imaging phenotype experimentally relates to disease clinically. As MRI is now a cornerstone of both animal studies and patient research, it forms a vital methodological link between basic research and clinical implementation.

## Acknowledgements

This work was supported by the Canadian Institutes of Health Research, the Natural Sciences and Engineering Research Council of Canada, Alberta Innovates — Health Solutions, the Multiple Sclerosis Society of Canada, and the Alberta endMS Regional Research and Training Centre of the endMS Research and Training Network.

## References

Aboul-Enein, F., Krssak, M., Hoftberger, R., Prayer, D., Kristoferitsch, W., 2010. Reduced NAA-levels in the NAWM of patients with MS is a feature of progression. A study with quantitative magnetic resonance spectroscopy at 3 Tesla. PloS One 5 (7), e11625. http://dx.doi.org/10.1371/journal.pone.0011625, 20652023.

Adams, C.W., 1988. Perivascular iron deposition and other vascular damage in multiple sclerosis. Journal of Neurology, Neurosurgery, and Psychiatry 51 (2), 260–5. http://dx.doi.org/10.1136/jnnp.51.2.260, 3346691.

Adams, R.D., Kubik, C.S., 1952. The morbid anatomy of the demyelinative disease. American Journal of Medicine 12 (5), 510–46. http://dx.doi.org/10.1016/0002-9343(52)90234-9, 14933429.

Agrawal, S., Anderson, P., Durbeej, M., van Rooijen, N., Ivars, F., Opdenakker, G., et al. 2006. Dystroglycan is selectively cleaved at the parenchymal basement membrane at sites of leukocyte extravasation in experimental autoimmune encephalomyelitis. Journal of Experimental Medicine 203 (4), 1007–19. http://dx.doi.org/10.1084/jem.20051342, 16585265.

Agrawal, S.M., Silva, C., Tourtellotte, W.W., Yong, V.W., 2011. EMMPRIN: a novel regulator of leukocyte transmigration into the CNS in multiple sclerosis and experimental autoimmune encephalomyelitis. Journal of Neuroscience: the Official Journal of the Society for Neuroscience 31 (2), 669–77. http://dx.doi.org/10.1523/JNEUROSCI.3659-10.2011, 21228176.

Aharoni, R., Sasson, E., Blumenfeld-Katzir, T., Eilam, R., Sela, M., Assaf, Y., et al. 2013. Magnetic resonance imaging characterization of different experimental autoimmune encephalomyelitis models and the therapeutic effect of glatiramer acetate. Experimental Neurology 240C, 130–44, 23153580.

Anderson, S.A., Shukaliak-Quandt, J., Jordan, E.K., Arbab, A.S., Martin, R., McFarland, H., et al. 2004. Magnetic resonance imaging of labeled T-cells in a mouse model of multiple sclerosis. Annals of Neurology 55 (5), 654–9. http://dx.doi.org/10.1002/ana.20066, 15122705.

Baeten, K., Adriaensens, P., Hendriks, J., Theunissen, E., Gelan, J., Hellings, N., et al. 2010. Tracking of myelin-reactive T cells in experimental autoimmune encephalomyelitis (EAE) animals using small particles of iron oxide and MRI. NMR in Biomedicine 23 (6), 601–9. http://dx.doi.org/10.1002/nbm.1501, 20661874.

Baeten, K., Hendriks, J.J., Hellings, N., Theunissen, E., Vanderlocht, J., Ryck, L.D., et al. 2008. Visualisation of the kinetics of macrophage infiltration during experimental autoimmune encephalomyelitis by magnetic resonance imaging. Journal of Neuroimmunology 195 (1–2), 1–6. http://dx.doi.org/10.1016/j.jneuroim.2007.11.008, 18177950.

Bagnato, F., Jeffries, N., Richert, N.D., Stone, R.D., Ohayon, J.M., McFarland, H.F., et al. 2003. Evolution of T1 black holes in patients with multiple sclerosis imaged monthly for 4 years. Brain: A Journal of Neurology 126 (8), 1782–9. http://dx.doi.org/10.1093/brain/awg182, 12821527.

Barkhof, F., Filippi, M., Miller, D.H., Scheltens, P., Campi, A., Polman, C.H., et al. 1997. Comparison of MRI criteria at first presentation to predict conversion to clinically definite multiple sclerosis. Brain: A Journal of Neurology 120 (11), 2059–69. http://dx.doi.org/10.1093/brain/120.11.2059, 9397021.

Battistini, L., Piccio, L., Rossi, B., Bach, S., Galgani, S., Gasperini, C., et al. 2003. CD8+ T cells from patients with acute multiple sclerosis display selective increase of adhesiveness in brain venules: a critical role for P-selectin glycoprotein ligand-1. Blood 101 (12), 4775–82, 12595306.

Baxter, A.G., 2007. The origin and application of experimental autoimmune encephalomyelitis. Nat. Revue d'Immunologie 7 (11), 904–12. http://dx.doi.org/10.1038/nri2190.

Bendszus, M., Ladewig, G., Jestaedt, L., Misselwitz, B., Solymosi, L., Toyka, K., et al. 2008. Gadofluorine M enhancement allows more sensitive detection of inflammatory CNS lesions than T2-w imaging: a quantitative MRI study. Brain: A Journal of Neurology 131 (9), 2341–52. http://dx.doi.org/10.1093/brain/awn156, 18669504.

Blakemore, W.F., 1973. Demyelination of the superior cerebellar peduncle in the mouse induced by cuprizone. Journal of the Neurological Sciences 20 (1), 63–72. http://dx.doi.org/10.1016/0022-510X(73)90118-4, 4744511.

Blakemore, W.F., 1978. Observations on remyelination in the rabbit spinal cord following demyelination induced by lysolecithin. Neuropathology and Applied Neurobiology 4 (1), 47–59, 683458.

Blezer, E.L., Bauer, J., Brok, H.P., Nicolay, K., Hart, T., 2007. Quantitative MRI-pathology correlations of brain white matter lesions developing in a non-human primate model of multiple sclerosis. NMR in Biomedicine 20 (2), 90–103. http://dx.doi.org/10.1002/nbm.1085, 16948176.

Boretius, S., Escher, A., Dallenga, T., Wrzos, C., Tammer, R., Bruck, W., et al. 2012. Assessment of lesion pathology in a new animal model of MS by multiparametric MRI and DTI. Neuroimage 59 (3), 2678–88. http://dx.doi.org/10.1016/j.neuroimage.2011.08.051, 21914485.

Boretius, S., Schmelting, B., Watanabe, T., Merkler, D., Tammer, R., Czeh, B., et al. 2006. Monitoring of EAE onset and progression in the common marmoset monkey by sequential high-resolution 3D MRI. NMR in Biomedicine 19 (1), 41–9. http://dx.doi.org/10.1002/nbm.999, 16408325.

Brenner, R.E., Munro, P.M., Williams, S.C., Bell, J.D., Barker, G.J., Hawkins, C.P., et al. 1993. The proton NMR spectrum in acute EAE: the significance of the change in the Cho:Cr ratio. Magnetic Resonance in Medicine: Official Journal of the Society of Magnetic Resonance in Medicine / Society of Magnetic Resonance in Medicine 29 (6), 737–45. http://dx.doi.org/10.1002/mrm.1910290605, 8350716.

Brochet, B., Deloire, M.S., Touil, T., Anne, O., Caille, J.M., Dousset, V., et al. 2006. Early macrophage MRI of inflammatory lesions predicts lesion severity and disease development in relapsing EAE. NeuroImage 32 (1), 266–74. http://dx.doi.org/10.1016/j.neuroimage.2006.03.028, 16650776.

Budde, M.D., Kim, J.H., Liang, H.F., Russell, J.H., Cross, A.H., Song, S.K., 2008. Axonal injury detected by in vivo diffusion tensor imaging correlates with neurological disability in a mouse model of multiple sclerosis. NMR in Biomedicine 21 (6), 589–97. http://dx.doi.org/10.1002/nbm.1229, 18041806.

Budde, M.D., Xie, M., Cross, A.H., Song, S.K., 2009. Axial diffusivity is the primary correlate of axonal injury in the experimental autoimmune encephalomyelitis spinal cord: a quantitative pixelwise analysis. Journal of Neuroscience: the Official Journal of the Society for Neuroscience 29 (9), 2805–13. http://dx.doi.org/10.1523/JNEUROSCI.4605-08.2009, 19261876.

Buenz, E.J., Sauer, B.M., Lafrance-Corey, R.G., Deb, C., Denic, A., German, C.L., et al. 2009. Apoptosis of hippocampal pyramidal neurons is virus independent in a mouse model of acute neurovirulent picornavirus infection. American Journal of Pathology 175 (2), 668–84. http://dx.doi.org/10.2353/ajpath.2009.081126, 19608874.

Cannella, B., Cross, A.H., Raine, C.S., 1990. Upregulation and coexpression of adhesion molecules correlate with relapsing autoimmune demyelination in the central nervous system. Journal of Experimental Medicine 172 (5), 1521–4. http://dx.doi.org/10.1084/jem.172.5.1521, 2172438.

Cannella, B., Raine, C.S., 1995. The adhesion molecule and cytokine profile of multiple sclerosis lesions. Annals of Neurology 37 (4), 424–35. http://dx.doi.org/10.1002/ana.410370404, 7536402.

Ceccarelli, A., Rocca, M.A., Valsasina, P., Rodegher, M., Falini, A., Comi, G., et al. 2010. Structural and functional magnetic resonance imaging correlates of motor network dysfunction in primary progressive multiple sclerosis. European Journal of Neuroscience 31 (7), 1273–80. http://dx.doi.org/10.1111/j.1460-9568.2010.07147.x, 20345920.

Chen, C.C., Zechariah, A., Hsu, Y.H., Chen, H.W., Yang, L.C., Chang, C., 2008. Neuroaxonal ion dyshomeostasis of the normal-appearing corpus callosum in experimental autoimmune encephalomyelitis. Experimental Neurology 210 (2), 322–30. http://dx.doi.org/10.1016/j.expneurol.2007.11.008, 18201701.

Chin, C.L., Pai, M., Bousquet, P.F., Schwartz, A.J., O'Connor, E.M., Nelson, C.M., et al. 2009. Distinct spatiotemporal pattern of CNS lesions revealed by USPIO-enhanced MRI in MOG-induced EAE rats implicates the involvement of spino-olivocerebellar pathways. Journal of Neuroimmunology 211 (1–2), 49–55. http://dx.doi.org/10.1016/j.jneuroim.2009.03.012, 19346009.

Cook, L.L., Foster, P.J., Karlik, S.J., 2005. Pathology-guided MR analysis of acute and chronic experimental allergic encephalomyelitis spinal cord lesions at 1.5 T. Journal of Magnetic Resonance Imaging: JMRI 22 (2), 180–8. http://dx.doi.org/10.1002/jmri.20368, 16028251.

Dal, Canto M.C., Kim, B.S., Miller, S.D., Melvold, R.W., 1996. Theiler's murine encephalomyelitis virus (TMEV)-induced demyelination: a model for human multiple sclerosis. Methods (San Diego, Calif.) 10 (3), 453–61. http://dx.doi.org/10.1006/meth.1996.0123, 8954856.

Dal, Canto M.C., Lipton, H.L., 1975. Primary demyelination in Theiler's virus infection. An ultrastructural study. Laboratory Investigation; a Journal of Technical Methods and Pathology 33 (6), 626–37, 1202282.

DeBoy, C.A., Zhang, J., Dike, S., Shats, I., Jones, M., Reich, D.S., et al. 2007. High resolution diffusion tensor imaging of axonal damage in focal inflammatory and demyelinating lesions in rat spinal cord. Brain: A Journal of Neurology 130 (8), 2199–210. http://dx.doi.org/10.1093/brain/awm122, 17557778.

Degaonkar, M.N., Jayasundar, R., Jagannathan, N.R., 2002. Sequential diffusion-weighted magnetic resonance imaging study of lysophosphatidyl choline-induced experimental demyelinating lesion: an animal model of multiple sclerosis. Journal of Magnetic Resonance Imaging: JMRI 16 (2), 153–9. http://dx.doi.org/10.1002/jmri.10143, 12203762.

Deloire-Grassin, M.S., Brochet, B., Quesson, B., Delalande, C., Dousset, V., Canioni, P., et al. 2000. In vivo evaluation of remyelination in rat brain by magnetization transfer imaging. Journal of the Neurological Sciences 178 (1), 10–16. http://dx.doi.org/10.1016/S0022-510X(00)00331-2, 11018243.

Denic, A., Johnson, A.J., Bieber, A.J., Warrington, A.E., Rodriguez, M., Pirko, I., 2011. The relevance of animal models in multiple sclerosis research. Pathophysiology: the Official Journal of the International Society for Pathophysiology / ISP 18 (1), 21–9, 20537877.

Dousset, V., Ballarino, L., Delalande, C., Coussemacq, M., Canioni, P., Petry, K.G., et al. 1999. Comparison of ultrasmall particles of iron oxide (USPIO)-enhanced T2-weighted, conventional T2-weighted, and gadolinium-enhanced T1-weighted MR images in rats with experimental autoimmune encephalomyelitis. AJNR. American Journal of Neuroradiology 20 (2), 223–7, 10094342.

Dousset, V., Brochet, B., Deloire, M.S., Lagoarde, L., Barroso, B., Caille, J.M., et al. 2006. MR imaging of relapsing multiple sclerosis patients using ultra-small-particle iron oxide and compared with gadolinium. AJNR. American Journal of Neuroradiology 27 (5), 1000–5, 16687532.

Dousset, V., Brochet, B., Vital, A., Gross, C., Benazzouz, A., Boullerne, A., et al. 1995. Lysolecithin-induced demyelination in primates: preliminary in vivo study with MR and magnetization transfer. AJNR. American Journal of Neuroradiology 16 (2), 225–31, 7726066.

Dousset, V., Delalande, C., Ballarino, L., Quesson, B., Seilhan, D., Coussemacq, M., et al. 1999. In vivo macrophage activity imaging in the central nervous system detected by magnetic resonance. Magnetic Resonance in Medicine: Official Journal of the Society of Magnetic Resonance in Medicine / Society of Magnetic Resonance in Medicine 41 (2), 329–33. http://dx.doi.org/10.1002/(SICI)1522-2594(199902)41:2<329::AID-MRM17>3.0.CO;2-Z, 10080281.

Dousset, V., Grossman, R.I., Ramer, K.N., Schnall, M.D., Young, L.H., Gonzalez-Scarano, F., et al. 1992. Experimental allergic encephalomyelitis and multiple sclerosis: lesion characterization with magnetization transfer imaging. Radiology 182 (2), 483–91, 1732968.

Ebers, G.C., 1985. Optic neuritis and multiple sclerosis. Archives of Neurology 42 (7), 702–4. http://dx.doi.org/10.1001/archneur.1985.04060070096025, 4015469.

Engberink, R.D., van, der Pol S.M., Walczak, P., van, der Toorn A., Viergever, M.A., Dijkstra, C.D., et al. 2010. Magnetic resonance imaging of monocytes labeled with ultrasmall superparamagnetic particles of iron oxide using magnetoelectroporation in an animal model of multiple sclerosis. Molecular Imaging 9 (5), 268–77, 20868627.

Enriquez-Algeciras, M., Ding, D., Chou, T.H., Wang, J., Padgett, K.R., Porciatti, V., et al. 2011. Evaluation of a transgenic mouse model of multiple sclerosis with noninvasive methods. Investigative Ophthalmology & Visual Science 52 (5), 2405–11. http://dx.doi.org/10.1167/iovs.10-6425, 21228378.

Filippi, M., Rocca, M.A., 2011. MR imaging of multiple sclerosis. Radiology 259 (3), 659–81. http://dx.doi.org/10.1148/radiol.11101362, 21602503.

Fisher, E., Lee, J.C., Nakamura, K., Rudick, R.A., 2008. Gray matter atrophy in multiple sclerosis: a longitudinal study. Annals of Neurology 64 (3), 255–65. http://dx.doi.org/10.1002/ana.21436, 18661561.

Fjaer, S., Bo, L., Lundervold, A., Myhr, K.M., Pavlin, T., Torkildsen, O., et al. 2013. Deep gray matter demyelination detected by magnetization transfer ratio in the cuprizone model. PLOS One 8 (12), e84162. http://dx.doi.org/10.1371/journal.pone.0084162, 24386344.

Floris, S., Blezer, E.L., Schreibelt, G., Dopp, E., van, der Pol S.M., Schadee-Eestermans, I.L., et al. 2004. Blood–brain barrier permeability and monocyte infiltration in experimental allergic encephalomyelitis: a quantitative MRI study. Brain: A Journal of Neurology 127 (3), 616–27, 14691063.

Ford, C.C., Ceckler, T.L., Karp, J., Herndon, R.M., 1990. Magnetic resonance imaging of experimental demyelinating lesions. Magnetic Resonance in Medicine: Official Journal of the Society of Magnetic Resonance in Medicine / Society of Magnetic Resonance in Medicine 14 (3), 461–81. http://dx.doi.org/10.1002/mrm.1910140305, 2355829.

Gareau, P.J., Rutt, B.K., Karlik, S.J., Mitchell, J.R., 2000. Magnetization transfer and multicomponent T2 relaxation measurements with histopathologic correlation in an experimental model of MS. Journal of Magnetic Resonance Imaging: JMRI 11 (6), 586–95. http://dx.doi.org/10.1002/1522-2586(200006)11:6<586::AID-JMRI3>3.0.CO;2-V, 10862056.

Harrison, D.M., Shiee, N., Bazin, P.L., Newsome, S.D., Ratchford, J.N., Pham, D., et al. 2013. Tract-specific quantitative MRI better correlates with disability than conventional MRI in multiple sclerosis. Journal of Neurology 260 (2), 397–406, 22886062.

Hart, B.A., Bauer, J., Muller, H.J., Melchers, B., Nicolay, K., Brok, H., et al. 1998. Histopathological characterization of magnetic resonance imaging-detectable brain white matter lesions in a primate model of multiple sclerosis: a correlative study in the experimental autoimmune encephalomyelitis model in common marmosets (*Callithrix jacchus*). American Journal of Pathology 153 (2), 649–63. http://dx.doi.org/10.1016/S0002-9440(10)65606-4, 9708823.

Hawkins, C.P., Munro, P.M., MacKenzie, F., Kesselring, J., Tofts, P.S., du Boulay, E.P., et al. 1990. Duration and selectivity of blood–brain barrier breakdown in chronic relapsing experimental allergic encephalomyelitis studied by gadolinium–DTPA and protein markers. Brain: A Journal of Neurology 113 (2), 365–78, 2328409.

Hopp, K., Popescu, B.F., McCrea, R.P., Harder, S.L., Robinson, C.A., Haacke, M.E., et al. 2010. Brain iron detected by SWI high pass filtered phase calibrated with synchrotron X-ray fluorescence. Journal of Magnetic Resonance Imaging: JMRI 31 (6), 1346–54. http://dx.doi.org/10.1002/jmri.22201, 20512886.

Husted, C.A., Goodin, D.S., Hugg, J.W., Maudsley, A.A., Tsuruda, J.S., de Bie, S.H., et al. 1994. Biochemical alterations in multiple sclerosis lesions and normal-appearing white matter detected by in vivo $^{31}$P and $^{1}$H spectroscopic imaging. Annals of Neurology 36 (2), 157–65. http://dx.doi.org/10.1002/ana.410360207, 8053651.

Inglese, M., Li, B.S., Rusinek, H., Babb, J.S., Grossman, R.I., Gonen, O., 2003. Diffusely elevated cerebral choline and creatine in relapsing–remitting multiple sclerosis. Magnetic Resonance in Medicine: Official Journal of the Society of Magnetic Resonance in Medicine / Society of Magnetic Resonance in Medicine 50 (1), 190–5. http://dx.doi.org/10.1002/mrm.10481, 12815694.

Karlik, S.J., Gilbert, J.J., Wong, C., Vandervoort, M.K., Noseworthy, J.H., 1990. NMR studies in experimental allergic encephalomyelitis: factors which contribute to T1 and T2 values. Magnetic Resonance in Medicine: Official Journal of the Society of Magnetic Resonance in Medicine / Society of Magnetic Resonance in Medicine 14 (1), 1–11. http://dx.doi.org/10.1002/mrm.1910140102, 1693744.

Karlik, S.J., Grant, E.A., Lee, D., Noseworthy, J.H., 1993. Gadolinium enhancement in acute

and chronic-progressive experimental allergic encephalomyelitis in the guinea pig. Magnetic Resonance in Medicine: Official Journal of the Society of Magnetic Resonance in Medicine / Society of Magnetic Resonance in Medicine 30 (3), 326–31. http://dx.doi.org/10.1002/mrm.1910300308, 8412603.

Khalil, M., Enzinger, C., Langkammer, C., Tscherner, M., Wallner-Blazek, M., Jehna, M., et al. 2009. Quantitative assessment of brain iron by R(2)* relaxometry in patients with clinically isolated syndrome and relapsing–remitting multiple sclerosis. Multiple Sclerosis (Houndmills, Basingstoke, England) 15 (9), 1048–54. http://dx.doi.org/10.1177/1352458509106609, 19556316.

Kipp, M., Van, Der Star B., Vogel, D.Y.S., Puentes, F., Van, Der Valk P., Baker, D., et al. 2012. Experimental in vivo and in vitro models of multiple sclerosis: EAE and beyond. Multiple Sclerosis and Related Disorders 1 (1), 15–28.

Kolbe, S., Chapman, C., Nguyen, T., Bajraszewski, C., Johnston, L., Kean, M., et al. 2009. Optic nerve diffusion changes and atrophy jointly predict visual dysfunction after optic neuritis. Neuroimage 45 (3), 679–86. http://dx.doi.org/10.1016/j.neuroimage.2008.12.047, 19162205.

Kuharik, M.A., Edwards, M.K., Farlow, M.R., Becker, G.J., Azzarelli, B., Klatte, E.C., et al. 1988. Gd-enhanced MR imaging of acute and chronic experimental demyelinating lesions. AJNR. American Journal of Neuroradiology 9 (4), 643–8, 3135711.

Ladewig, G., Jestaedt, L., Misselwitz, B., Solymosi, L., Toyka, K., Bendszus, M., et al. 2009. Spatial diversity of blood–brain barrier alteration and macrophage invasion in experimental autoimmune encephalomyelitis: a comparative MRI study. Experimental Neurology 220 (1), 207–11. http://dx.doi.org/10.1016/j.expneurol.2009.08.027, 19733560.

Laule, C., Vavasour, I.M., Moore, G.R., Oger, J., Li, D.K., Paty, D.W., et al. 2004. Water content and myelin water fraction in multiple sclerosis. A T2 relaxation study. Journal of Neurology 251 (3), 284–93. http://dx.doi.org/10.1007/s00415-004-0306-6, 15015007.

Lee, J., Shmueli, K., Kang, B.T., Yao, B., Fukunaga, M., van Gelderen, P., et al. 2012. The contribution of myelin to magnetic susceptibility-weighted contrasts in high-field MRI of the brain. Neuroimage 59 (4), 3967–75. http://dx.doi.org/10.1016/j.neuroimage.2011.10.076, 22056461.

Lin, A., Ross, B.D., Harris, K., Wong, W., 2005. Efficacy of proton magnetic resonance spectroscopy in neurological diagnosis and neurotherapeutic decision making. NeuroRx: the Journal of the American Society for Experimental NeuroTherapeutics 2 (2), 197–214. http://dx.doi.org/10.1602/neurorx.2.2.197, 15897945.

Liu, Y., Duan, Y., He, Y., Yu, C., Wang, J., Huang, J., et al. 2012. Whole brain white matter changes revealed by multiple diffusion metrics in multiple sclerosis: a TBSS study. European Journal of Radiology 81 (10), 2826–32, 22172535.

MacKenzie-Graham, A., Rinek, G.A., Avedisian, A., Gold, S.M., Frew, A.J., Aguilar, C., et al. 2012. Cortical atrophy in experimental autoimmune encephalomyelitis: in vivo imaging. Neuroimage 60 (1), 95–104. http://dx.doi.org/10.1016/j.neuroimage.2011.11.099, 22182769.

MacKenzie-Graham, A., Tinsley, M.R., Shah, K.P., Aguilar, C., Strickland, L.V., Boline, J., et al. 2006. Cerebellar cortical atrophy in experimental autoimmune encephalomyelitis. NeuroImage 32 (3), 1016–23. http://dx.doi.org/10.1016/j.neuroimage.2006.05.006, 16806982.

MacKenzie-Graham, A., Tiwari-Woodruff, S.K., Sharma, G., Aguilar, C., Vo, K.T., Strickland, L.V., et al. 2009. Purkinje cell loss in experimental autoimmune encephalomyelitis. Neuroimage 48 (4), 637–51. http://dx.doi.org/10.1016/j.neuroimage.2009.06.073, 19589388.

Macmillan, C.J., Starkey, R.J., Easton, A.S., 2011. Angiogenesis is regulated by angiopoietins during experimental autoimmune encephalomyelitis and is indirectly related to vascular permeability. Journal of Neuropathology and Experimental Neurology 70 (12), 1107–23. http://dx.doi.org/10.1097/NEN.0b013e31823a8b6a, 22082662.

Mastronardi, F.G., Ackerley, C.A., Arsenault, L., Roots, B.I., Moscarello, M.A., 1993. Demyelination in a transgenic mouse: a model for multiple sclerosis. Journal of Neuroscience Research 36 (3), 315–24. http://dx.doi.org/10.1002/jnr.490360309, 7505836.

Matsushima, G.K., Morell, P., 2001. The neurotoxicant, cuprizone, as a model to study demyelination and remyelination in the central nervous system. Brain Pathology (Zurich, Switzerland) 11 (1), 107–16, 11145196.

McCreary, C.R., Bjarnason, T.A., Skihar, V., Mitchell, J.R., Yong, V.W., Dunn, J.F., 2009. Multiexponential T2 and magnetization transfer MRI of demyelination and remyelination in murine spinal cord. Neuroimage 45 (4), 1173–82. http://dx.doi.org/10.1016/j.neuroimage.2008.12.071, 19349232.

Merkler, D., Boretius, S., Stadelmann, C., Ernsting, T., Michaelis, T., Frahm, J., et al. 2005. Multicontrast MRI of remyelination in the central nervous system. NMR in Biomedicine 18 (6), 395–403. http://dx.doi.org/10.1002/nbm.972, 16086436.

Millward, J.M., Schnorr, J., Taupitz, M., Wagner, S., Wuerfel, J.T., Infante-Duarte, C., 2013. Iron oxide magnetic nanoparticles highlight early involvement of the choroid plexus in central nervous system inflammation. ASN Neuro 5 (1), e00110, 23452162.

Minderhoud, J.M., Mooyaart, E.L., Kamman, R.L., Teelken, A.W., Hoogstraten, M.C., Vencken, L.M., et al. 1992. In vivo phosphorus magnetic resonance spectroscopy in multiple sclerosis. Archives of Neurology 49 (2), 161–5. http://dx.doi.org/10.1001/archneur.1992.00530260063021, 1736849.

Mistry, N., Dixon, J., Tallantyre, E., Tench, C., Abdel-Fahim, R., Jaspan, T., et al. 2013. Central veins in brain lesions visualized with high-field magnetic resonance imaging: a pathologically specific diagnostic biomarker for inflammatory demyelination in the Brain. JAMA Neurology **70** (, 623–8, 23529352.

Mori, Y., Murakami, M., Arima, Y., Zhu, D., Terayama, Y., Komai, Y., et al. 2014. Early pathological alterations of lower lumbar cords detected by ultrahigh-field MRI in a mouse multiple sclerosis model. International Immunology 26 (2), 93–101, 24150245.

Naismith, R.T., Xu, J., Tutlam, N.T., Scully, P.T., Trinkaus, K., Snyder, A.Z., et al. 2010. Increased diffusivity in acute multiple sclerosis lesions predicts risk of black hole. Neurology 74 (21), 1694–701. http://dx.doi.org/10.1212/WNL.0b013e3181e042c4, 20498437.

Nathoo, N., Agrawal, S., Wu, Y., Haylock-Jacobs, S., Yong, V.W., Foniok, T., et al. 2013. Susceptibility-weighted imaging in the experimental autoimmune encephalomyelitis model of multiple sclerosis indicates elevated deoxyhemoglobin, iron deposition and demyelination. Multiple Sclerosis (Houndmills, Basingstoke, England) 19 (6), 721–31. http://dx.doi.org/10.1177/1352458512460602, 23027879.

Nathoo, N., Jeong, D., Foniok, T., Keough, M.B., Yong, V.W., Dunn, J.F., 2013. Diffusion Tensor Tractography Identifies Demyelination and Remyelination in the Spinal Cord of a Mouse Model of Multiple Sclerosis. Salt Lake City, UT, USA: International Society for Magnetic Resonance in Medicine.

Nathoo, N., Yong, V.W., Dunn, J.F., 2014. Using magnetic resonance imaging in animal models to guide drug development in multiple sclerosis. Multiple Sclerosis (Houndmills, Basingstoke, England) 20 (1), 3–11, 24263386.

Nessler, S., Boretius, S., Stadelmann, C., Bittner, A., Merkler, D., Hartung, H.P., et al. 2007. Early MRI changes in a mouse model of multiple sclerosis are predictive of severe inflammatory tissue damage. Brain 130 (8), 2186–98. http://dx.doi.org/10.1093/brain/awm105.

O'Brien, J.T., Noseworthy, J.H., Gilbert, J.J., Karlik, S.J., 1987. NMR changes in experimental allergic encephalomyelitis: NMR changes precede clinical and pathological events. Magnetic Resonance in Medicine: Official Journal of the Society of Magnetic Resonance in Medicine / Society of Magnetic Resonance in Medicine 5 (2), 109–17. http://dx.doi.org/10.1002/mrm.1910050203, 3657500.

Optic Neuritis Study Group 2008. Multiple sclerosis risk after optic neuritis: final optic neuritis treatment trial follow-up. Archives of Neurology 65 (6), 727–32, 18541792.

Oweida, A.J., Dunn, E.A., Karlik, S.J., Dekaban, G.A., Foster, P.J., 2007. Iron-oxide labeling of hematogenous macrophages in a model of experimental autoimmune encephalomyelitis and the contribution to signal loss in fast imaging employing steady state acquisition (FIESTA) images. Journal of Magnetic Resonance Imaging: JMRI 26 (1), 144–51. http://dx.doi.org/10.1002/jmri.21005, 17659552.

Pirko, I., Ciric, B., Johnson, A.J., Gamez, J., Rodriguez, M., Macura, S., 2003. Magnetic resonance imaging of immune cells in inflammation of central nervous system. Croatian Medical Journal 44 (4), 463–8, 12950151.

Pirko, I., Gamez, J., Johnson, A.J., Macura, S.I., Rodriguez, M., 2004. Dynamics of MRI lesion development in an animal model of viral-induced acute progressive CNS demyelination. NeuroImage 21 (2), 576–82. http://dx.doi.org/10.1016/j.neuroimage.2003.09.037, 14980559.

Pirko, I., Johnson, A., Ciric, B., Gamez, J., Macura, S.I., Pease, L.R., et al. 2004. In vivo magnetic resonance imaging of immune cells in the central nervous system with superparamagnetic antibodies. FASEB Journal: Official Publication of the Federation of American Societies for Experimental Biology 18 (1), 179–82, 14630708.

Pirko, I., Johnson, A., Gamez, J., Macura, S.I., Rodriguez, M., 2004. Disappearing "T1 black holes" in an animal model of multiple sclerosis. Frontiers in Bioscience: A Journal and Virtual Library 9, 1222–7. http://dx.doi.org/10.2741/1322, 14977539.

Pirko, I., Johnson, A.J., Chen, Y., Lindquist, D.M., Lohrey, A.K., Ying, J., et al. 2011. Brain atrophy correlates with functional outcome in a murine model of multiple sclerosis. Neuroimage 54 (2), 802–6. http://dx.doi.org/10.1016/j.neuroimage.2010.08.055, 20817104.

Pirko, I., Johnson, A.J., Lohrey, A.K., Chen, Y., Ying, J., 2009. Deep gray matter T2 hypointensity correlates with disability in a murine model of MS. Journal of the Neurological Sciences 282 (1–2), 34–8. http://dx.doi.org/10.1016/j.jns.2008.12.013, 19162280.

Pirko, I., Nolan, T.K., Holland, S.K., Johnson, A.J., 2008. Multiple sclerosis: pathogenesis and MR imaging features of T1 hypointensities in a [corrected] murine model. Radiology 246 (3), 790–5. http://dx.doi.org/10.1148/radiol.2463070338, 18309014.

Polman, C.H., Reingold, S.C., Banwell, B., Clanet, M., Cohen, J.A., Filippi, M., et al. 2011. Diagnostic criteria for multiple sclerosis: 2010 revisions to the McDonald criteria. Annals of Neurology 69 (2), 292–302. http://dx.doi.org/10.1002/ana.22366, 21387374.

Preece, N.E., Baker, D., Butter, C., Gadian, D.G., Urenjak, J., 1993. Experimental allergic encephalomyelitis raises betaine levels in the spinal cord of strain 13 guinea-pigs. NMR in Biomedicine 6 (3), 194–200. http://dx.doi.org/10.1002/nbm.1940060305, 8347453.

Ransohoff, R.M., 2012. Animal models of multiple sclerosis: the good, the bad and the bottom line. Nature Neuroscience 15 (8), 1074–7. http://dx.doi.org/10.1038/nn.3168, 22837037.

Rausch, M., Hiestand, P., Baumann, D., Cannet, C., Rudin, M., 2003. MRI-based monitoring of inflammation and tissue damage in acute and chronic relapsing EAE. Magnetic Resonance in Medicine: Official Journal of the Society of Magnetic Resonance in Medicine / Society of Magnetic Resonance in Medicine 50 (2), 309–14. http://dx.doi.org/10.1002/mrm.10541, 12876707.

Rausch, M., Tofts, P., Lervik, P., Walmsley, A., Mir, A., Schubart, A., et al. 2009. Characterization of white matter damage in animal models of multiple sclerosis by magnetization transfer ratio and quantitative mapping of the apparent bound proton fraction f. Multiple Sclerosis (Houndmills, Basingstoke, England) 15 (1), 16–27, 18971220.

Richards, T.L., Alvord, E.C. Jr., Peterson, J., Cosgrove, S., Petersen, R., Petersen, K., et al. 1995. Experimental allergic encephalomyelitis in non-human primates: MRI and MRS may predict the type of brain damage. NMR in Biomedicine 8 (2), 49–58. http://dx.doi.org/10.1002/nbm.1940080202, 7547186.

Rigotti, D.J., Inglese, M., Kirov, I.I., Gorynski, E., Perry, N.N., Babb, J.S., et al. 2012. Two-year serial whole-brain N-acetyl-l-aspartate in patients with relapsing–remitting multiple sclerosis. Neurology 78 (18), 1383–9. http://dx.doi.org/10.1212/WNL.0b013e318253d609, 22517095.

Robinson, K.M., Njus, J.M., Phillips, D.A., Proctor, T.M., Rooney, W.D., Jones, R.E., 2010. MR imaging of inflammation during myelin-specific T cell-mediated autoimmune attack in the EAE mouse spinal cord. Molecular Imaging and Biology: MIB: the Official Publication of the Academy of Molecular Imaging 12 (3), 240–9. http://dx.doi.org/10.1007/s11307-009-0272-6, 19949987.

Sahraian, M.A., Radue, E.W., Haller, S., Kappos, L., 2010. Black holes in multiple sclerosis: definition, evolution, and clinical correlations. Acta Neurologica Scandinavica 122 (1), 1–8, 20003089.

Schellenberg, A.E., Buist, R., Yong, V.W., Del, Bigio M.R., Peeling, J., 2007. Magnetic resonance imaging of blood–spinal cord barrier disruption in mice with experimental autoimmune encephalomyelitis. Magnetic Resonance in Medicine: Official Journal of the Society of Magnetic Resonance in Medicine / Society of Magnetic Resonance in Medicine 58 (2), 298–305. http://dx.doi.org/10.1002/mrm.21289, 17654586.

Schmierer, K., Scaravilli, F., Altmann, D.R., Barker, G.J., Miller, D.H., 2004. Magnetization transfer ratio and myelin in postmortem multiple sclerosis brain. Annals of Neurology 56 (3), 407–15. http://dx.doi.org/10.1002/ana.20202, 15349868.

Serres, S., Mardiguian, S., Campbell, S.J., McAteer, M.A., Akhtar, A., Krapitchev, A., et al. 2011. VCAM-1-targeted magnetic resonance imaging reveals subclinical disease in a mouse model of multiple sclerosis. FASEB Journal: Official Publication of the Federation of American Societies for Experimental Biology 25 (12), 4415–22. http://dx.doi.org/10.1096/fj.11-183772, 21908714.

Silva, A.C., Bock, N.A., 2008. Manganese-enhanced MRI: an exceptional tool in translational neuroimaging. Schizophrenia Bulletin 34 (4), 595–604, 18550591.

Sipkins, D.A., Gijbels, K., Tropper, F.D., Bednarski, M., Li, K.C., Steinman, L., 2000. ICAM-1 expression in autoimmune encephalitis visualized using magnetic resonance imaging. Journal of Neuroimmunology 104 (1), 1–9. http://dx.doi.org/10.1016/S0165-5728(99)00248-9, 10683508.

Skripuletz, T., Lindner, M., Kotsiari, A., Garde, N., Fokuhl, J., Linsmeier, F., et al. 2008. Cortical demyelination is prominent in the murine cuprizone model and is strain-dependent. American Journal of Pathology 172 (4), 1053–61. http://dx.doi.org/10.2353/ajpath.2008.070850, 18349131.

Smorodchenko, A., Wuerfel, J., Pohl, E.E., Vogt, J., Tysiak, E., Glumm, R., et al. 2007. CNS-irrelevant T-cells enter the brain, cause blood–brain barrier disruption but no glial pathology. European Journal of Neuroscience 26 (6), 1387–98. http://dx.doi.org/10.1111/j.1460-9568.2007.05792.x, 17880383.

Song, S.K., Yoshino, J., Le, T.Q., Lin, S.J., Sun, S.W., Cross, A.H., et al. 2005. Demyelination increases radial diffusivity in corpus callosum of mouse brain. NeuroImage 26 (1), 132–40. http://dx.doi.org/10.1016/j.neuroimage.2005.01.028, 15862213.

Steffen, B.J., Butcher, E.C., Engelhardt, B., 1994. Evidence for involvement of ICAM-1 and VCAM-1 in lymphocyte interaction with endothelium in experimental autoimmune encephalomyelitis in the central nervous system in the SJL/J mouse. American Journal of Pathology 145 (1), 189–201, 7518194.

Steinman, L., Zamvil, S.S., 2005. Virtues and pitfalls of EAE for the development of therapies for multiple sclerosis. Trends in Immunology 26 (11), 565–71. http://dx.doi.org/10.1016/j.it.2005.08.014, 16153891.

Stepp, S.E., Mathew, P.A., Bennett, M., de, Saint Basile G., Kumar, V., 2000. Perforin: More than just an effector molecule. Immunology Today 21 (6), 254–6. http://dx.doi.org/10.1016/S0167-5699(00)01622-4, 10825735.

Stewart, W.A., Alvord, E.C. Jr., Hruby, S., Hall, L.D., Paty, D.W., 1991. Magnetic resonance imaging of experimental allergic encephalomyelitis in primates. Brain: A Journal of Neurology 114 (2), 1069–96. http://dx.doi.org/10.1093/brain/114.2.1069, 2043942.

Stoll, G., Kleinschnitz, C., Meuth, S.G., Braeuninger, S., Ip, C.W., Wessig, C., et al. 2009. Transient widespread blood–brain barrier alterations after cerebral photothrombosis as revealed by gadofluorine M-enhanced magnetic resonance imaging. Journal of Cerebral Blood Flow and Metabolism: Official Journal of the International Society of Cerebral Blood Flow and Metabolism 29 (2), 331–41. http://dx.doi.org/10.1038/jcbfm.2008.129, 18957988.

Sun, S.W., Liang, H.F., Schmidt, R.E., Cross, A.H., Song, S.K., 2007. Selective vulnerability of cerebral white matter in a murine model of multiple sclerosis detected using diffusion tensor imaging. Neurobiology of Disease 28 (1), 30–8, 17683944.

Sun, S.W., Liang, H.F., Trinkaus, K., Cross, A.H., Armstrong, R.C., Song, S.K., 2006. Non-invasive detection of cuprizone induced axonal damage and demyelination in the mouse corpus callosum. Magnetic Resonance in Medicine: Official Journal of the Society of Magnetic Resonance in Medicine / Society of Magnetic Resonance in Medicine 55 (2), 302–8. http://dx.doi.org/10.1002/mrm.20774, 16408263.

Tartaglia, M.C., Narayanan, S., De, Stefano N., Arnaoutelis, R., Antel, S.B., Francis, S.J., et al. 2002. Choline is increased in pre-lesional normal appearing white matter in multiple sclerosis. Journal of Neurology 249 (10), 1382–90. http://dx.doi.org/10.1007/s00415-002-0846-6, 12382153.

Tedeschi, G., Lavorgna, L., Russo, P., Prinster, A., Dinacci, D., Savettieri, G., et al. 2005. Brain atrophy and lesion load in a large population of patients with multiple sclerosis. Neurology 65 (2), 280–5. http://dx.doi.org/10.1212/01.wnl.0000168837.87351.1f, 16043800.

Thiessen, J.D., Zhang, Y., Zhang, H., Wang, L., Buist, R., Del, Bigio M.R., et al. 2013. Quantitative MRI and ultrastructural examination of the cuprizone mouse model of demyelination. NMR in Biomedicine 26 (11), 1562–81. http://dx.doi.org/10.1002/nbm.2992, 23943390.

Tillema, J.M., Leach, J., Pirko, I., 2012. Non-lesional white matter changes in pediatric multiple sclerosis and monophasic demyelinating disorders. Multiple Sclerosis (Houndmills, Basingstoke, England) 18 (12), 1754–9. http://dx.doi.org/10.1177/1352458512447527, 22641299.

Tourdias, T., Mori, N., Dragonu, I., Cassagno, N., Boiziau, C., Aussudre, J., et al. 2011. Differential aquaporin 4 expression during edema build-up and resolution phases of brain inflammation. Journal of Neuroinflammation 8, 143. http://dx.doi.org/10.1186/1742-2094-8-143, 22011386.

Tourdias, T., Roggerone, S., Filippi, M., Kanagaki, M., Rovaris, M., Miller, D.H., et al. 2012. Assessment of disease activity in multiple sclerosis phenotypes with combined gadolinium- and superparamagnetic iron oxide-enhanced MR imaging. Radiology 264 (1), 225–33. http://dx.doi.org/10.1148/radiol.12111416, 22723563.

Trapp, B.D., Ransohoff, R., Rudick, R., 1999. Axonal pathology in multiple sclerosis: relationship to neurologic disability. Current Opinion in Neurology 12 (3), 295–302, 10499174.

Trip, S.A., Wheeler-Kingshott, C., Jones, S.J., Li, W.Y., Barker, G.J., Thompson, A.J., et al. 2006. Optic nerve diffusion tensor imaging in optic neuritis. NeuroImage 30 (2), 498–505. http://dx.doi.org/10.1016/j.neuroimage.2005.09.024, 16242968.

Tysiak, E., Asbach, P., Aktas, O., Waiczies, H., Smyth, M., Schnorr, J., et al. 2009. Beyond blood brain barrier breakdown — in vivo detection of occult neuroinflammatory foci by magnetic nanoparticles in high field MRI. Journal of Neuroinflammation 6, 20. http://dx.doi.org/10.1186/1742-2094-6-20, 19660125.

Vellinga, M.M., Oude, Engberink R.D., Seewann, A., Pouwels, P.J., Wattjes, M.P., van, der Pol S.M., et al. 2008. Pluriformity of inflammation in multiple sclerosis shown by ultra-small iron oxide particle enhancement. Brain: A Journal of Neurology 131 (3), 800–7. http://dx.doi.org/10.1093/brain/awn009, 18245785.

Vercellino, M., Masera, S., Lorenzatti, M., Condello, C., Merola, A., Mattioda, A., et al. 2009. Demyelination, inflammation, and neurodegeneration in multiple sclerosis deep gray matter. Journal of Neuropathology and Experimental Neurology 68 (5), 489–502. http://dx.doi.org/10.1097/NEN.0b013e3181a19a5a, 19525897.

Verhoye, M.R., Gravenmade, E.J., Raman, E.R., Van Reempts, J., Van, der Linden A., 1996. In vivo noninvasive determination of abnormal water diffusion in the rat brain studied in an animal model for multiple sclerosis by diffusion-weighted NMR imaging. Magnetic Resonance Imaging 14 (5), 521–32. http://dx.doi.org/10.1016/0730-725X(96)00047-1, 8843364.

Waiczies, H., Millward, J.M., Lepore, S., Infante-Duarte, C., Pohlmann, A., Niendorf, T., et al. 2012. Identification of cellular infiltrates during early stages of brain inflammation with magnetic resonance microscopy. PloS One 7 (3), e32796. http://dx.doi.org/10.1371/journal.pone.0032796, 22427887.

Walsh, A.J., Lebel, R.M., Eissa, A., Blevins, G., Catz, I., Lu, J.Q., et al. 2013. Multiple sclerosis: validation of MR imaging for quantification and detection of Iron. Radiology 267 (2), 531–42. http://dx.doi.org/10.1148/radiol.12120863, 23297322.

Wang, Y., Wang, Q., Haldar, J.P., Yeh, F.C., Xie, M., Sun, P., et al. 2011. Quantification of increased cellularity during inflammatory demyelination. Brain: A Journal of Neurology 134 (12), 3590–601. http://dx.doi.org/10.1093/brain/awr307, 22171354.

Wu, Q.Z., Yang, Q., Cate, H.S., Kemper, D., Binder, M., Wang, H.X., et al. 2008. MRI identification of the rostral–caudal pattern of pathology within the corpus callosum in the cuprizone mouse model. Journal of Magnetic Resonance Imaging: JMRI 27 (3), 446–53. http://dx.doi.org/10.1002/jmri.21111, 17968901.

Wuerfel, E., Infante-Duarte, C., Glumm, R., Wuerfel, J.T., 2010. Gadofluorine M-enhanced MRI shows involvement of circumventricular organs in neuroinflammation. Journal of Neuroinflammation 7, 70. http://dx.doi.org/10.1186/1742-2094-7-70, 20955604.

Wuerfel, J., Tysiak, E., Prozorovski, T., Smyth, M., Mueller, S., Schnorr, J., et al. 2007. Mouse model mimics multiple sclerosis in the clinico-radiological paradox. European Journal of Neuroscience 26 (1), 190–8. http://dx.doi.org/10.1111/j.1460-9568.2007.05644.x, 17596194.

Xie, M., Tobin, J.E., Budde, M.D., Chen, C.I., Trinkaus, K., Cross, A.H., et al. 2010. Rostrocaudal analysis of corpus callosum demyelination and axon damage across disease stages refines diffusion tensor imaging correlations with pathological features. Journal of Neuropathology and Experimental Neurology 69 (7), 704–16. http://dx.doi.org/10.1097/NEN.0b013e3181e3de90, 20535036.

Xu, S., Jordan, E.K., Brocke, S., Bulte, J.W., Quigley, L., Tresser, N., et al. 1998. Study of relapsing remitting experimental allergic encephalomyelitis SJL mouse model using MION-46L enhanced in vivo MRI: early histopathological correlation. Journal of Neuroscience Research 52 (5), 549–58. http://dx.doi.org/10.1002/(SICI)1097-4547(19980601)52:5%3C549::AID-JNR7%3E3.3.CO;2-6, 9632311.

Zaaraoui, W., Deloire, M., Merle, M., Girard, C., Raffard, G., Biran, M., et al. 2008. Monitoring demyelination and remyelination by magnetization transfer imaging in the mouse brain at 9.4 T. Magma (New York, N.Y.) 21 (5), 357–62. http://dx.doi.org/10.1007/s10334-008-0141-3, 18779984.

Zhang, J., Jones, M.V., McMahon, M.T., Mori, S., Calabresi, P.A., 2012. In vivo and ex vivo diffusion tensor imaging of cuprizone-induced demyelination in the mouse corpus callosum. Magnetic Resonance in Medicine: Official Journal of the Society of Magnetic Resonance in Medicine / Society of Magnetic Resonance in Medicine 67 (3), 750–9. http://dx.doi.org/10.1002/mrm.23032, 21656567.

Zhang, Y., Traboulsee, A., Zhao, Y., Metz, L.M., Li, D.K., 2011. Texture analysis differentiates persistent and transient T1 black holes at acute onset in multiple sclerosis: a preliminary study. Multiple Sclerosis (Houndmills, Basingstoke, England) 17 (5), 532–40. http://dx.doi.org/10.1177/1352458510395981, 21270058.